

Intrinsic and Synaptic Mechanisms Determining the Timing of Neuron Population Activity During Hippocampal Theta Oscillation

Gergő Orbán,^{1,2} Tamás Kiss,^{1,3} and Péter Érdi^{1,3}

¹Department of Biophysics, KFKI Research Institute for Particle and Nuclear Physics, Hungarian Academy of Sciences, Budapest;

²Collegium Budapest, Institute for Advanced Study; Budapest, Hungary; and ³Center for Complex Systems Studies, Kalamazoo College, Kalamazoo, Michigan

Submitted 23 November 2006; accepted in final form 20 July 2006

Orbán, Gergő, Tamás Kiss, and Péter Érdi. Intrinsic and synaptic mechanisms determining the timing of neuron population activity during hippocampal theta oscillation. *J Neurophysiol* 96: 2889–2904, 2006. First published August 9, 2006; doi:10.1152/jn.01233.2005. Hippocampal theta (3–8 Hz) is a major electrophysiological activity in rodents, which can be found in primates and humans as well. During theta activity, pyramidal cells and different classes of interneurons were shown to discharge at different phases of the extracellular theta. A recent in vitro study has shown that theta-frequency oscillation can be elicited in a hippocampal CA1 slice by the activation of metabotropic glutamate receptors with similar pharmacological and physiological profile that was found in vivo. We constructed a conductance based three-population network model of the hippocampal CA1 region to study the specific roles of neuron types in the generation of the in vitro theta oscillation and the emergent network properties. Interactions between pairs of neuron populations were studied systematically to assess synchronization and delay properties. We showed that the circuitry consisting of pyramidal cells and two types of hippocampal interneurons [basket and oriens lacunosum-moleculare (O-LM) neurons] was able to generate coherent theta-frequency population oscillation. Furthermore, we found that hyperpolarization-activated nonspecific cation current in pyramidal cells, but not in O-LM neurons, plays an important role in the timing of spike generation, and thus synchronization of pyramidal cells. The model was shown to exhibit the same phase differences between neuron population activities found in vivo, supporting the idea that these patterns of activity are determined internal to the hippocampus.

INTRODUCTION

Hippocampal theta activity (3–8 Hz) is known to involve multiple cell populations (Buzsáki 2002; Vértes and Kocsis 1997) and was shown to be synchronized over spatial scales ≤ 2 mm (Bullock et al. 1990). Synchronization of theta activity was suggested to be brought about by extrinsic (Alonso et al. 1987; Mitchell and Ranck 1980; Petsche et al. 1962) and intrinsic mechanisms (Chapman and Lacaille 1999; Kocsis et al. 1999; Strata 1998). Although the septal pacemaker hypothesis is supported by both physiological (Bland et al. 1999) and computational (Wang 2002) studies, producing a coherent hippocampal theta might require additional mechanisms (Buzsáki 2002; King et al. 1998). Importantly, intracellular equivalent of theta oscillation was identified in individual CA1 neurons in the form of subthreshold oscillations, and activity of these neurons was also modulated by theta activity (Soltész and

Deschenes 1993). The subthreshold oscillation was proven to be carried by rhythmic GABA_A inhibitory postsynaptic potentials (IPSPs) (Ylinen et al. 1995). Further studies showed that pharmacological modulation of GABA_A receptors was shown to alter hippocampal theta in vivo (Hajós et al. 2004; Ongini et al. 1983). Recently, it has been shown in vivo that different neuron populations tend to fire at different phases of extracellularly measured theta (Csicsvári et al. 1999; Skaggs et al. 1996), and interneuron subclasses proved to be distinguishable based on their preferred action potential timing relative to theta (Klausberger et al. 2003, 2004). The question whether and how intrinsic mechanisms contribute to the synchronization of hippocampal neuron populations in the theta frequency band remains open.

The view that external input paces the firing of neuron populations is supported by their anatomical organization (Freund and Buzsáki 1996; Pawelzik et al. 2002), enabling them to collect afferents from the entorhinal cortex and, in the case of CA1, the CA3 region of the hippocampus. The idea of internal modulation of firing patterns is supported by physiological properties of hippocampal interneurons that might underlie the relay of fast feedback inhibition subserving pyramidal cells synchronization (Jonas et al. 2004). Also, an internal effect in the hippocampus is the intrinsic resonance of pyramidal cells to theta-frequency periodic inputs (Strata 1998). Furthermore, a recent in vitro study has shown that theta could be elicited in a CA1 slice (Gillies et al. 2002), and timing of different neuronal classes was similar to those measured in vivo. Taken together, these studies indicate that patterning of hippocampal neuron population activities has to rely on the anatomical organization and dynamics of the hippocampus.

Preferential discharge of basket cells, whose primary target is the perisomatic region of pyramidal cells (Freund and Buzsáki 1996), precedes that of pyramidal cells by 60 ms (Klausberger et al. 2003). The timing of pyramidal cell firing by basket cells was previously suggested by Buzsáki et al. (1983) and Fox (1989), but the precise mechanism remained to be elucidated. A possible mechanism of pyramidal cell timing was given by Cobb et al. (1995), who revealed a postinhibitory “rebound depolarization” in the membrane potential traces of CA1 pyramidal cells but intrinsic currents responsible for the phenomenon were not identified.

Pharmacological profile of theta activity poses constraints on plausible mechanisms underlying its generation. During ket-

Address for reprint requests and other correspondence: G. Orbán, Dept. Biophysics, KFKI Research Inst. for Particle and Nuclear Physics, Hungarian Acad. of Sciences, 29-33 Konkoly-Thege M. út, Budapest H-1121, Hungary (E-mail: ogergo@sunserv.kfki.hu).

The costs of publication of this article were defrayed in part by the payment of page charges. The article must therefore be hereby marked “advertisement” in accordance with 18 U.S.C. Section 1734 solely to indicate this fact.

amine and urethane anesthesia, theta was proven to be atropine sensitive, whereas theta measured in behaving animals does not show this property (Vanderwolf et al. 1988). Carbachol models of theta activity rely on the activation of muscarinic receptors (Williams and Kauer 1997) therefore are sensitive to atropine. However, the *in vitro* theta elicited by activation of metabotropic glutamate receptors was shown to be atropine resistant (Gillies et al. 2002). Furthermore, similar to *in vivo* models (Buzsáki 2002), this model was shown to depend on intact *N*-methyl-D-aspartate (NMDA) transmission and blockade of GABA_A also attenuated the extracellularly measured theta oscillation. An additional characteristic feature of this *in vitro* model was its sensitivity to the blockade of the hyperpolarization-activated current (I_h). Although it is known that I_h is present in multiple cell populations, including pyramidal (Magee 1998) and oriens lacunosum-moleculare interneurons (O-LM cells) (Maccaferri and McBain 1996), the identity of those effectively contributing to the generation of theta was not determined. Also, blockade of I_h was found to disrupt firing of O-LM cells in CA1 (Gillies et al. 2002). O-LM cells are prone targets of the recurrent axons of pyramidal neurons. Their discharge is in an almost perfect overlap with that of pyramidal cells in the hippocampal CA1 region. The question therefore is how O-LM neurons contribute to the dependence of hippocampal theta activity on glutamatergic transmission components.

We used compartmental modeling techniques to study the conditions necessary for the emergence of theta oscillation in the hippocampal CA1 circuitry. The main objective was the study of processes that set the firing phase differences of neuron populations participating in theta oscillation. We used a three-population intrahippocampal network model of area CA1 and aimed at providing a mechanism of the *in vitro* model of atropine-resistant theta oscillations (Gillies et al. 2002). First, we explored the properties of interactions between neuron populations and revealed that nonlinearity realized by the activation of I_h channels is effective in the precise timing of pyramidal cell firing. Second, we examined the properties of theta oscillations and showed that delay relationships between firing of neuron populations relied on intrahippocampal interactions. Third, we examined the pharmacological profile of the population oscillation, showing the role that I_h and glutamate receptors possibly play.

METHODS

Both pyramidal cells and a number of interneuron subtypes, including basket cells, axo-axonic cells, O-LM interneurons, and bistratified cells were shown to have firing patterns phase locked to theta oscillation (Klausberger et al. 2003, 2004). In addition, lacunosum-moleculare interneurons were shown to exhibit slow intrinsic periodic spiking (2–5 Hz) as well (Chapman and Lacaille 1999). From the great variety of these cell types, we confined our study to those that are likely to participate in feedback inhibition of pyramidal cells. Based on their location and the termination pattern of recurrent collaterals, basket cells and O-LM cells were taken into account. The computational model of hippocampal CA1 consisted of three neuron populations including pyramidal neurons and two types of interneurons: O-LM cells and basket interneurons. Computer simulations used conductance based model neurons described by the Hodgkin-Huxley formalism.

Neuron types

The multicompartmental pyramidal cell model was an extended version of the 256 compartmental model of Warman et al. (1994). The original model contained seven types of ionic currents: sodium (I_{Na}), delayed rectifier potassium (I_K), A-type potassium ($I_{K(A)}$), muscarinic potassium ($I_{K(M)}$), C-type potassium ($I_{K(C)}$), low threshold calcium (I_{Ca}), and calcium concentration-dependent potassium ($I_{K(AHP)}$). In addition to the originally implemented currents, we added hyperpolarization-activated nonspecific cation current (I_h). I_h channels are confined to the dendritic regions of pyramidal cells; therefore studying the effects of I_h on somatic firing necessitated the usage of a multicompartmental model. Distribution and kinetic parameters of I_h channels were set according to the data provided in the paper of Magee (1998). The I_h current was described by equations of the standard Hodgkin-Huxley formalism: $I_h = g_h h(V_m - E_h)$, where g_h was the maximal synaptic conductance, and E_h was the reversal potential of the current. Maximal conductance of I_h was 10 pS/cm² at the soma and increased linearly as a function of the distance from the soma reaching a maximum at the most distal apical dendrites of 100 pS/cm². The reversal potential was set to 0 mV. The gating variable h was described by first-order kinetics, in the form of $dh/dt = [h_\infty(V) - h]/\tau_h(V)$. Values for $h_\infty(V)$ and $\tau_h(V)$ were fitted on data by Magee (1998).

Pyramidal cells received a constant depolarizing current, which was injected in their somata. Strength of this depolarization varied from cell to cell and was picked from a Gaussian distribution. Width of the Gaussian was typically set to 30 pA. Mean level of the tonic depolarizing current varied between 0 and 700 pA and was 600 pA if not stated otherwise.

Basket neurons formed the fast spiking neuron population of the pyramidal layer. The single-compartmental model contained only two active currents: I_{Na} and I_K (Orbán et al. 2001; Wang and Buzsáki 1996). Gate speed variable Φ was set to 2. A constant depolarizing current was given to each basket neuron, whose level was 1.4 μ A/cm² throughout the simulations. Firing frequency of the uncoupled neurons was 81 Hz. The cell surface was set to be equal to the area of a sphere with a radius of 20 μ m.

O-LM interneurons represented one of those interneuron populations whose somata resided in the oriens/alveus border. Besides I_{Na} and I_K , the single-compartmental model featured high-threshold calcium, hyperpolarization-activated potassium, and hyperpolarization activated mixed cation currents (Wang 2002). The O-LM neuron was able to generate repetitive action potentials autonomously. For the regulation of the firing rates of O-LM neurons, we occasionally added a constant hyperpolarizing or depolarizing current, but its default value was 0 μ A/cm². Firing frequency of neurons without synaptic input was 4.9 Hz. In addition, heterogeneity of O-LM cells was introduced by adding a tonic hyperpolarizing current to each cell heterogeneously and setting its level according to a Gaussian distribution. SD of the distribution was 0.07 μ A/cm² on Figs. 5, 6H, and 7. Spatial dimensions were the same as used for the basket neurons.

Neuron population size in network simulations was 100, 70, and 15, respectively, for basket neurons, O-LM cells, and pyramidal neurons in Figs. 6, 7B, and 9, whereas the number of O-LM cells was 30 in Fig. 5. Results were also tested with a network consisting of 200 basket cells, 90 O-LM cells, and varied number of pyramidal cells; an example of simulations with 30 pyramidal neurons is shown in Fig. 7A. Increasing the number of O-LM cells while keeping convergence-divergence levels constant did not result in significant changes in the activity of pyramidal cells; thus we did not study this factor. Using a lower number of pyramidal cells in the model is justified by the sparse recurrent collaterals in the CA1 region of the hippocampus.

Synapses and connectivity patterns

Synaptic contacts were either inhibitory or excitatory (Fig. 1). At each neuron population, postsynaptic neurons were selected ran-

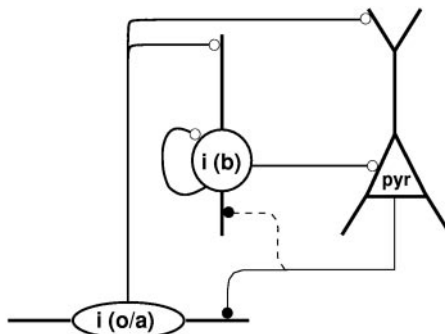


FIG. 1. Skeleton of the network used in our model. Pyr, pyramidal cell; i(b), basket neuron; i(o/a), oriens lacunosum-moleculare (O-LM) neuron. Solid lines represent connections between the neuron populations synapses are represented by circles (empty and filled circles stand for inhibitory and excitatory synapses, respectively). Pyramidal cell to basket cell connections (dashed line) are only effective on Fig. 9.

domly; therefore the spatial aspects of synaptization were ignored. Synaptic contacts established by pyramidal cells were glutamatergic. In most simulations, only NMDA receptor-mediated transmission was used, but in several simulations, α -amino-3-hydroxy-5-methyl-4-isoxazolepropionic acid (AMPA) receptor-mediated excitatory postsynaptic potentials were also taken into account (Fig. 9). Both AMPA and NMDA synapses obeyed first-order kinetics (Destexhe et al. 1998). We modified the original model of NMDA synapse by changing the parameters determining the magnesium dependency of the NMDA channel (Kuner and Schoepfer 1996): $b([Mg^{2+}]) = 1/(1 + \exp(vV/[Mg^2]/\eta))$, with $v = -41 \text{ mV}^{-1}$, $\eta = 1.57 \text{ mM}$, and $[Mg^{2+}] = 2 \text{ mM}$.

Synapses established by interneurons were inhibitory and were mediated by GABA_A receptors. Synaptic current was in the standard form of $I_{\text{syn}} = g_{\text{syn}}s(V - E_{\text{syn}})$, where the activation variable s obeyed first-order kinetics $ds/dt = \alpha F(V_{\text{pre}})(1 - s) - \beta s$ (Wang and Buzsáki 1996). In the previous equation, $F(V_{\text{pre}})$ was described by $F(V_{\text{pre}}) = 1/1 + \exp[-(V_{\text{pre}} - \Theta_{\text{syn}})/K]$. Parameters characterizing synaptic contacts between neurons were as follows: for basket-to-pyramidal cell and O-LM cell-to-pyramidal cell connections: $\alpha = 10 \text{ ms}^{-1}$, $\beta = 0.07 \text{ ms}^{-1}$, $K = 2 \text{ mV}$, $E_{\text{syn}} = -80 \text{ mV}$; for basket-to-basket cell connections: $\alpha = 10 \text{ ms}^{-1}$, $\beta = 0.07 \text{ ms}^{-1}$, $K = 2 \text{ mV}$, $E_{\text{syn}} = -75 \text{ mV}$; for O-LM cell-to-basket cell connections, the decay was slower (Hájos and Mody 1997): $\alpha = 20 \text{ ms}^{-1}$, $\beta = 0.05 \text{ ms}^{-1}$, $K = 0.5 \text{ mV}$, $E_{\text{syn}} = -80 \text{ mV}$. Release threshold Θ_{syn} was set to 0 mV at each GABA_A synapse.

For each cell type, the pattern of synaptic contacts was random: convergence and divergence were set, whereas pre- and postsynaptic neurons were selected randomly. Throughout the paper, convergence numbers denote the exact number of efferent synapses on a single neuron, and similarly, divergence numbers denote the exact number of target neurons a neuron is innervating. Magnitudes of synaptic conductances for the established contacts were tested in a wide range; therefore both the ranges and default values (in parentheses) are given. Unless otherwise noted default values were used for figures shown throughout this paper. Synaptic strengths were set homogeneously for a given pair of pre-, and postsynaptic neuron population, no variance in the maximal synaptic conductance of individual contacts was introduced.

Recurrent collaterals of pyramidal cells are confined to the stratum oriens (Knowles et al. 1982) and are sparse in the CA1 region; therefore pyramidal cell-to-pyramidal cell connections were ignored. Pyramidal cells, however, provide the main excitatory input for oriens interneurons, including O-LM cells (Blasco-Ibanez and Freund 1995; Lacaille et al. 1987). Synaptic transmission was either mediated by NMDA receptors (Nyíri et al. 2003) or both NMDA and AMPA receptors (Baude et al. 1995; Nusser et al. 1998). Facilitation at these synapses was ignored (Ali and Thomson 1998). Each O-LM cell was

innervated by 1.6–5 pyramidal cells (default 2.4); maximal synaptic conductance was 0.5–1.1 nS (default 0.7 nS) at NMDA receptors and 1 nS at AMPA receptors. Pyramidal cells were shown to innervate basket neurons as well (Ali et al. 1998); therefore these connections were also implemented in our model. In these connections, however, NMDA receptor-mediated synaptic currents were not included as in the CA1 region of the hippocampus. NMDA receptor contacts were shown to be predominant on O-LM cells and less on parvalbumin positive, presumably basket, cells (Nyíri et al. 2003). Convergence of pyramidal cells was between 0 and 10 (default 0); maximal synaptic conductance of AMPA synapses was 1 nS.

O-LM cells projected to pyramidal cells (Gulyás et al. 1993a; McBain et al. 1994), establishing contacts through GABA_A receptor-mediated synapses. In addition, O-LM cells were shown to innervate interneurons as well (Katona et al. 1999), and interneurons with similar dendritic but different axonic arborization were shown to terminate on other local interneurons in the CA1 region (Gulyás et al. 2003). Although there is no data available on the physiological identity of these two types of interneurons, for simplicity, we used the same neuron population for the innervation of both pyramidal and basket neurons and used the term O-LM cells for these neurons. Convergence of O-LM neurons on pyramidal cells (Sík et al. 1995) was in the range of 8–20 (default 8) and was distributed on distal apical dendritic compartments on different branches of the dendritic tree. Maximal synaptic conductance was varied between 0.5 and 1.1 nS (default 0.88 nS). Convergence of O-LM neurons on basket cells (Katona et al. 1999) was in the range of 3 to 5 (default 5), whereas maximal synaptic conductance was 0.7–1.1 nS (default 0.88 nS).

Basket cells have axons largely confined to the stratum pyramidale and are known to form baskets on the somata of pyramidal cells. In the presented model, basket cells projected principally to the somata of pyramidal neurons (80%) and also terminated on the proximal apical dendrites (Freund and Buzsáki 1996; Sík et al. 1995). Convergence of basket cells on pyramidal cells was calculated from the divergence (Sík et al. 1995) and the relative number of the two cell types. Accordingly, convergence of basket cells on pyramidal cells varied between 10 and 30 (default was 20). However, the divergence of basket cells did not match the values obtained from experimental studies. As the pyramidal neuron was a multicompartmental implementation, it was not cost effective to have the same ratio of pyramidal cells and basket cells as would be in the case of an experimental situation. The low number of pyramidal cells was justified by the fact that recurrent collaterals are sparse in the CA1 region of the hippocampus (Lopes da Silva et al. 1990). Inhibitory synapses between basket cells and pyramidal cells were mediated by GABA_A receptors; maximal synaptic conductance was 0.7–1.4 nS (default 1.1 nS).

Parvalbumin containing putative basket neurons also have been shown to establish connections with other parvalbumin containing neurons (Sík et al. 1995). We set the divergence factor of basket cells according to this labeling study; thus a single basket neuron innervated 60 other basket cells on average. Maximal synaptic conductance was set to 0.25 nS.

When the network size was altered, convergences were kept constant to keep the depolarization level and thus average firing rates of individual cells unchanged. Table 1 shows a summary on connections among cell types.

Extracellular field potential

Population activity was characterized by an extracellular field potential, which was calculated using data obtained from pyramidal cells. The overwhelmingly larger number of pyramidal cells in the real neural tissue legitimized the method of using only pyramidal cell activity for this calculation. All simulated pyramidal cells were placed on the circumference of a 4 μm -radius circle and total transmembrane current in a compartment divided by the inverse of the distance of the respective compartment was summed for each compartment. Filtering

TABLE 1. Summary of synaptic connections in the model: type, convergence (c), and interval of maximal synaptic conductance (g_{max} given in pS) used in the simulations

	Pyramidal Cell	O-LM Cell	Basket Cell
Pyramidal cell	—	NMDA and AMPA $C = 1.6-5$ (2.4) $g_{max}^{AMPA} = 1$ $g_{max}^{NMDA} = 0.5-1.1$ (0.7)	AMPA $C = 0-10$ (0) $g_{max}^{AMPA} = 1$
O-LM cell	$GABA_A$ $C = 8-20$ (8) $g_{max}^{GABA} = 0.5-1.1$ (0.88)	—	$GABA_A$ $C = 3-5$ (5) $g_{max}^{GABA} = 0.7-1.1$ (0.88)
Basket cell	$GABA_A$ $C = 10-30$ (20) $g_{max}^{GABA} = 0.7-1.4$ (1.1)	—	$GABA_A$ $C = 60$ $g_{max}^{GABA} = 0.25$

Unless otherwise noted, values given in parentheses after intervals are used for simulations shown in figures. O-LM, Oriens lacunosum-moleculare; NMDA, *N*-methyl-D-aspartate; AMPA, α -amino-3-hydroxy-5-methyl-4-isoxazolepropionic acid.

properties of the extracellular medium was taken into account by low-pass filtering the signal (0–150 Hz), thus reducing the contribution of fast events to the EEG. Theta power was determined as the peak of the power spectrum of the EEG trace in the range of 3–8 Hz.

Integration time step was $1e-5$ s, and numerical integration was carried out with the Exponential Euler method. Initial conditions were random, and to provide an initial uniform distribution of pyramidal cell spikes, pyramidal cells were hyperpolarized for a time interval of length picked from a uniform distribution.

Simulations were performed with the GENESIS neural simulator program in Linux environment on a 16-node Beowulf cluster, also using the computational resources of the RMKI LCG center and the Hungarian ClusterGrid.

Data analysis

Reliability of disinhibition (R) was measured as the ratio of pyramidal cell spikes in a time window succeeding the beginning of disinhibition and total number of spikes fired during the simulation.

Disinhibition was achieved by the suppression of action potential firing of either a fraction or all neurons innervating the pyramidal cell, depending on the protocol. Suppression of presynaptic action potentials was a result of hyperpolarizing the presynaptic neurons in a short time interval. Disinhibition was delivered periodically (period is denoted by DP) for a given time length (DTW). Width of the time window used to determine R was one-tenth of DP. Reliability of disinhibition was calculated according to the formula

$$R = 100 \frac{\sum_{0 < t < 0.1DP} \text{No. spikes}}{\sum_{0 < t < DP} \text{No. spikes}}$$

(see also Fig. 2A).

PHASE DISTRIBUTION HISTOGRAMS. Preferred phase of a given cell's firing relative to a reference signal was analyzed, and histograms representing firing probability of individual cells as a function of phase of the reference signal were prepared. Reference signal was acquired from the hippocampal CA1 field potential by filtering it with

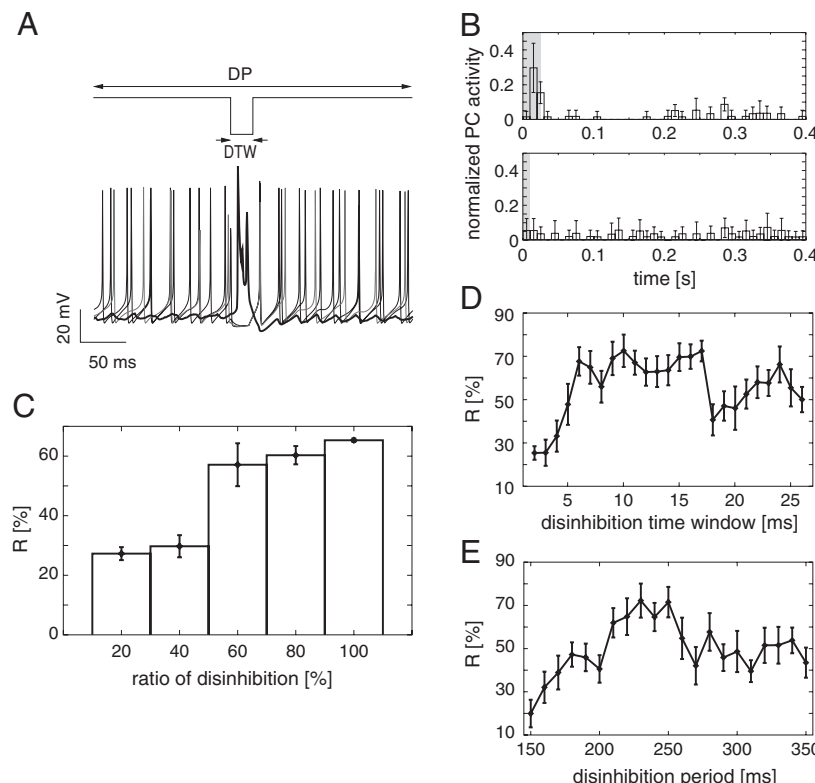


FIG. 2. Properties of pyramidal cell rebound spikes. A: protocol applied to test different parameters: a fraction of basket cells was silenced periodically [disinhibition period (DP)] by preventing their firing in a time window [disinhibition time window (DTW)]. Top: depolarizing current received by basket cells. Bottom: thick line: membrane potential (MP) of a pyramidal cell; thin lines, MPs of basket interneurons. B: 2 instances of pyramidal-burst distributions. Spike counts in a 10-ms time bin relative to spike number in a whole DP is plotted against time elapsed since beginning of the last DTW. Total number of basket cells inhibiting the pyramidal neuron was 20, maximal synaptic conductance was 2.9 nS, DP = 400 ms, and DTW = 25 and 10 ms for the top and bottom panel, respectively. Shaded areas denote time when pyramidal cell is disinhibited. C: reliability of disinhibition (R) as a function of fraction of silenced basket cells. Relative spike counts for the histograms were calculated from the 1st 30 ms after disinhibition. DTW = 25 ms, DP = 220 ms. D and E: changes in R with increasing width of DTW and increasing length of DP, respectively. At short inhibition periods reliability is low (E) and reliability does not increase with increasing window widths (D, gray line; DP 150 ms). At higher DPs (E) reliability reaches a maximum and converges to a constant value (in the range of investigated DPs). Initial low reliability increases with DTW and reaches a plateau at 7 ms in the case of high DP (D, black line; DP 220 ms). Ratio of disinhibition was 100% in both D and E and depolarization of the pyramidal cell was 0.6 nA in each simulation. Error bars denote SE.

a Gaussian filter. Phase (ϕ) of an action potential in degrees relative to the reference signal is calculated by the $\phi = 360^\circ(t - T_1)/(T_2 - T_1)$ equation, where t is the time of action potential occurrence, T_1 and T_2 are times of local maxima of the reference signal preceding and succeeding t , respectively.

The mean of phase distribution histograms was calculated by calculating circular mean of the histogram, in the form

$$\mu_p = P/2\pi(\arg\{\sum_{k=1}^N \exp[i2\pi\alpha(k)/P]\})_{2\pi}$$

where P denotes the period of the cycle, $\alpha(k)$ is the time of individual spikes and 2π in the index denotes modulo. Angular deviation was calculated as

$$\sigma_p = P/2\pi \sqrt{\sum_{k=1}^N (\arg\{\exp[i2\pi|\mu_p - \alpha(k)|/P]\})^2}$$

RESULTS

Conditions necessary for emergent theta activity in the hippocampal CA1 region were explored using a network of three distinct neuron types: pyramidal cells, O-LM cells, and basket neurons (see METHODS). Single cell properties and interactions between neuron populations setting the time scale of macroscopic population events were studied systematically. Because multiple neuron populations participate in theta activity in the hippocampus (Gillies et al. 2002), their interactions shape the population activity. To analyze the role individual cell populations and connections play in shaping the population activity and parameters individually testable, pairwise interactions between neuron populations were studied.

According to the scenario presented in our paper, recurrent collaterals of pyramidal cells excite O-LM neurons through NMDA receptor-mediated synapses, which excitation evokes action potentials in target neurons. Next, O-LM neurons inhibit a fraction of the basket cell population through GABA_A synapses. Synchronized inhibition partially suppresses firing of basket neurons, which in turn disinhibit target pyramidal cells, where slow I_h deactivation results in rebound action potentials in pyramidal cells.

In the following sections of RESULTS, components of this cycle were studied separately. In the first three sections, synaptic properties of the network were explored in pairwise interactions between basket neurons–pyramidal neurons; O-LM neurons–basket neurons; and pyramidal neurons–O-LM neurons, respectively. First, properties of basket cell–pyramidal cell coupling were explored to determine the conditions necessary for gating of pyramidal cell action potentials. Second, the modulation of basket cell firing rate by partially synchronous IPSPs was analyzed. Third, the synchronization properties of O-LM cells in response to phasic NMDA receptor-mediated input were analyzed. In the fourth section, we turn to the intrinsic properties of the pyramidal neuron enabling phasing of pyramidal cell activity by basket neurons. The role of hyperpolarization-activated current was analyzed in interpopulation interactions of basket and pyramidal cells by examining requirements of eliciting temporally precise rebound action potentials in pyramidal cells. Next, characteristics of theta oscillations were studied using the interconnected network of basket cells, O-LM cells, and pyramidal cells. Finally, contribution of glutamatergic transmission components and the hyperpolarization activated current to population oscillations were examined.

Reliability of pyramidal cell burst generation caused by disinhibition by basket neurons

It was previously shown in *in vitro* conditions that a sequence of fast IPSPs can synchronize pyramidal cell firing through the generation of a depolarizing overshoot in postsynaptic pyramidal neurons (Cobb et al. 1995). Because of the unique perisomatic location of basket cell synapses on pyramidal cells, these connections were regarded as key components in the timing of action potential generation. We studied the mechanism of how disinhibition of a pyramidal cell could result in rebound depolarization and finally in a rebound burst. For this, a randomly interconnected basket cell network was modeled, a fraction of which innervated the perisomatic region of a pyramidal neuron. In the presence of tonic depolarization basket cells provided rhythmic hyperpolarization of the pyramidal cell's soma through GABA_A-mediated IPSPs. Disinhibition of the target pyramidal cell was modeled by suppressing basket cell firing by manually giving a hyperpolarizing step current in a given time window (DTW; Fig. 2A). Suppression of basket cell firing was periodic (length of period is denoted by DP) resulting in periodic rebound burst generation by pyramidal cells. For a given experiment, pyramidal cell firing times relative to the disinhibition were averaged using multiple periods.

Suppressing basket cell action potentials often elicited bursts of action potentials at the target pyramidal neuron (Fig. 2A) but effectiveness of rebound burst generation showed considerable variability. Factors determining the reliability of disinhibition (R ; Fig. 2, A and B; also see METHODS) included the convergence of basket cells on pyramidal cells, the depth of basket cell modulation (i.e., number of suppressed basket cells), and the width of the disinhibition time window. Reliability of disinhibition increased with increasing number of innervating basket cells but saturated as a result of sublinear summation of IPSPs (data not shown). In the case when inhibition was only partially suppressed, that is, firing was only suppressed at a fraction of innervating basket cells, a clear decrease in R was observed (Fig. 2C). Reliability of disinhibition (R) rapidly increased when the ratio of disinhibited basket cells reached 60%, where R was $56 \pm 7\%$ (SE), meaning that the majority of pyramidal cell action potentials occurred immediately after disinhibition. *In vivo* data are available on such deep modulation of basket cells during theta activity (Klausberger et al. 2003), which promotes the plausibility of this mechanism to enable precise timing of pyramidal neurons.

Width of the DTW had little effect on R over a broad width range (Fig. 2D). Furthermore, disinhibition window width as short as ~ 10 ms proved to be sufficient to elicit postsynaptic response. This result also shows that high-frequency bombardment of the pyramidal cell was necessary for precise timing of postsynaptic pyramidal cells. At lower disinhibition period (DP; higher frequency), the reliability of disinhibition remained low, independent of the window width (Fig. 2D), indicating that broader disinhibition time window cannot compensate the large difference between disinhibition period and preferred frequency of the target neuron. Furthermore, a pyramidal neuron being subject to constant depolarizing current tends to generate bursts of action potentials with a certain frequency. This frequency also affects the effectiveness of periodical disinhibition. We

tested this effect by changing the disinhibition period instead of altering the frequency the pyramidal cell tends to fire with (2 Hz at 0.6-nA depolarizing current and 20 basket cells innervating the pyramidal cell). Reliability of disinhibition dropped seriously at small disinhibition periods and remained higher in an extended range after peaking at 230 ms (Fig. 2E). The result confirms that basket cells are able to set the timing of the model target pyramidal cell in an extended frequency range.

Modulation of basket cell network firing rate by synchronous IPSPs

Model O-LM interneurons established synaptic contacts with basket cells. We assumed a sparse connection between O-LM neurons and basket neurons (see METHODS) and studied

whether limited convergence of O-LM neurons on basket neurons can provide the suppression necessary for the effects shown in the previous section. Furthermore, we also checked whether periodically firing O-LM cells whose action potentials occur at dispersed phases can achieve similarly effective suppression of basket cells.

Simulations were performed with a population of O-LM neurons connected to a population of basket cells at various O-LM-to-basket cell divergence numbers and different maximal synaptic conductance at these synapses. Measures to quantify width and depth of inhibition of the basket cell population were set up (Fig. 3A). Two different protocols were used for the characterization of the interaction between the two cell populations. First, all O-LM neurons fired at the same time (Fig. 3, B and C), thus causing simultaneous inhibition of basket cells. Next, to model a more realistic scenario, O-LM

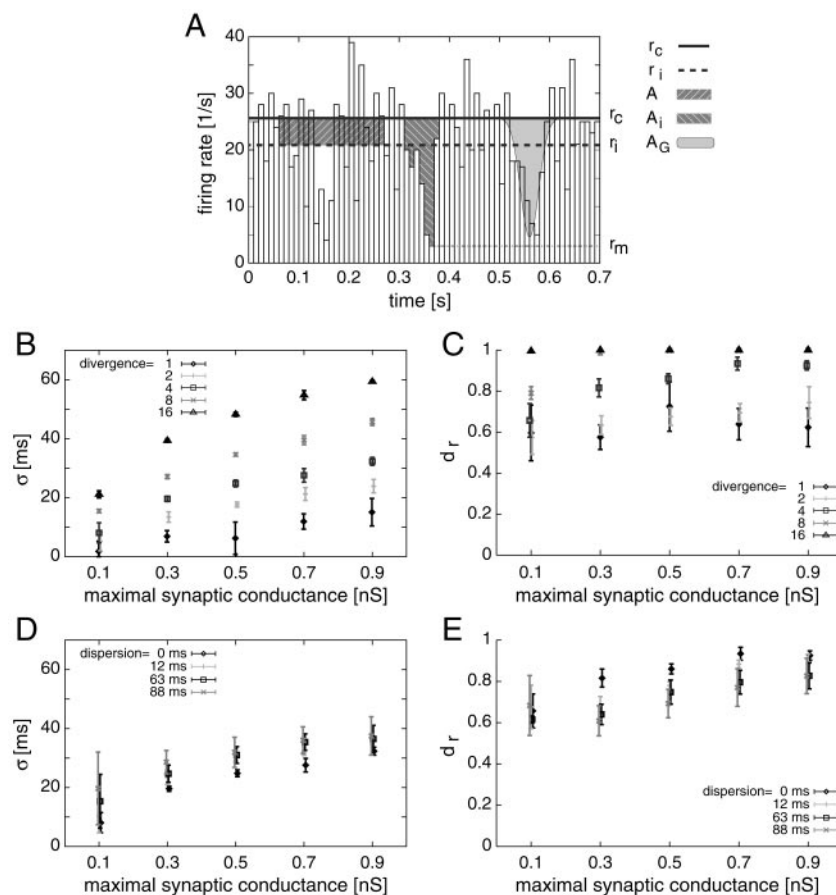


FIG. 3. Interaction between O-LM interneurons and basket cells. A: characterization of effect exerted by O-LM neurons on basket cells. Average firing rates were calculated for an isolated basket cell network (r_c , solid, thick line, $n = 100$, connection probability 60%) and for a basket cell network inhibited by the O-LM neurons (r_i , dashed, thick line). Decrease in average frequency of basket neurons indicates number of spikes that were suppressed by O-LM neurons. Because, under the provided conditions, O-LM cells generated action potentials in a strictly periodic manner (frequency was 4.79 Hz, period $T_{O-LM} = 209$ ms), during 1 period of O-LM cell firing, the number of suppressed basket cell spikes can be calculated as $A = nT_{O-LM}(r_c - r_i)$ (left-to-right dashed area). Spike histograms showing instantaneous firing rate of network were also calculated (bars). Area of depression in basket cell firing histogram was assumed to be equal to A (A_i , right-to-left dashed area) and was approximated by a Gaussian (A_G). Average depth of depression was calculated as the difference between the average isolated and average minimum rates ($d = r_c - r_m$). Width of depression was estimated by calculating the width of the Gaussian (gray shaded area): $\sigma = A/d\sqrt{1/\pi}$. Here, σ , A , and d are the width, area, and amplitude of the Gaussian, respectively. B and C: width and relative depth of depression as a function of O-LM to basket cell maximal synaptic conductance. Relative depth was calculated as ratio of average depth of depression to average firing rate in isolated basket cell network ($d_r = d/r_c$). Under provided conditions, all O-LM cells fired at the same time. O-LM to basket cell divergence numbers and maximal synaptic conductances were varied systematically. Both width and depth of depression increased with increasing synaptic strength. Width of depression fell below 5 ms in cases when both the divergence was small (<4) and maximal synaptic conductance was low (<0.3 nS). At high divergence levels (8 and above) depth of depression saturated. D and E: width and relative depth of depression at a fixed divergence (div = 4) but increasing variance of O-LM cell spike times. While width of depression increased with dispersed timing of O-LM neuron action potentials, relative depth of depression became smaller.

spiking times were set randomly: while individual O-LM neurons fired periodically, the firing phase of each neuron was set according to a Gaussian distribution with a given variance (Fig. 3, *D* and *E*). Simulations with simultaneous inhibition revealed that low convergence (as few as 4) was enough to modulate basket cell firing sufficiently for providing pyramidal cell disinhibition (Fig. 3*C*). Also, width of modulation has reached 10 ms for low convergence numbers and physiologically realistic synaptic strength (Fig. 3*B*). Nonsimultaneous inhibition increased the width of inhibition (Fig. 3*D*) and decreased the depth of inhibition (Fig. 3*E*), but conditions necessary to sufficiently suppress basket cell activity remained unchanged. Note, however, that with synchronous O-LM cell spikes (0-ms dispersion), the maximal depression was reached earlier than with dispersed spikes. At a maximal synaptic conductance of 0.5-nS delay of maximal depression, as measured from the mean of the firing times in the cluster of O-LM cell spikes, was 8.4 ± 1.2 ms at 0-ms dispersion, whereas at a dispersion of 63 ms, the delay was 21.2 ± 1.8 ms (histogram bin size was 200 ms). The fast suppression of basket cells shows that in the case of high O-LM cell synchrony the delay of basket cell suppression is mainly determined by the rise time of the IPSP.

Synchronization properties of the pyramidal cell–O-LM cell coupled oscillator system

Characteristics of phasic innervation of O-LM neurons by pyramidal cells were tested to determine the properties of NMDA receptor-mediated coupling. Synchronization between pyramidal cells and O-LM neurons was studied by simulations where one pyramidal cell innervated one O-LM interneuron through NMDA receptor-mediated synapse. Firing frequency of pyramidal cells and current injected into O-LM neurons were varied. In these simulations, O-LM cell to pyramidal cell feedback was not taken into account. As coupling is weak, synchronization is slow. Therefore we excluded initial transients by ignoring the first 1.5 s of the simulations. Time delays between pyramidal cell spikes and subsequent O-LM cell spikes were collected in a 5-s time interval, and their relative SD was calculated together with the ratio of number of O-LM cell spikes to the number of pyramidal cell spikes (Fig. 4). Small relative SD of spike time delays (dark regions on the figure) occurs in cases when the O-LM cell and the pyramidal cell fire synchronously. Simulations revealed that when depolarization did not drive O-LM cells to exhibit periodic firing behavior (below approximately -1.74 pA injected current; Fig. 4, *inset*), O-LM cell firing is 1:1 phase locked to pyramidal cell firing. When O-LM cells fire autonomously (injected current is more than approximately -1.74 pA), the period of O-LM cell firing doubles and then triples, whereas the first O-LM spike in a period follows the pyramidal cell spike after a constant time delay for a given pyramidal cell firing frequency. This relation is kept at ≤ 2 Hz pyramidal cell frequency. In this depolarization region, synchrony is maintained in narrow areas where period of O-LM cell oscillation is close to an integer multiple of the period of the pyramidal cell oscillation. In summary, even weak phasic NMDA coupling between pyramidal cells and O-LM neurons was capable of synchronizing O-LM cell firing to the action potentials of pyramidal cells.

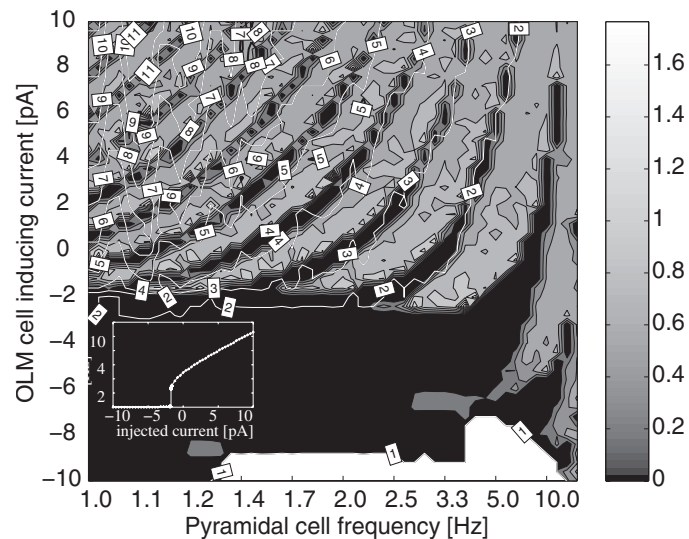


FIG. 4. Synchronization of O-LM cell and pyramidal cell firing. Firing frequency of the pyramidal cell and current injected into the O-LM neuron were varied. Time delays between each pyramidal cell spikes and subsequent O-LM neuron spikes were calculated for all pyramidal cell spikes in a 5-s time interval. Relative SD of these time delay values for pyramidal cell firing frequency—O-LM cell injected current pairs were plotted as gray shade map (in white area at bottom of image pyramidal cell firing could not evoke O-LM cell response). White contour lines with labels show the ratio of the number of O-LM cell spikes to number of pyramidal cell spikes. Maximal synaptic conductance was 0.7 nS as throughout other simulations. Firing of the O-LM cell and pyramidal cell is synchronized while injected current of O-LM interneurons is below threshold value where the O-LM cell start to generate action potentials autonomously and in narrow areas above this value. *Inset*: injected current vs. oscillation frequency of an isolated O-LM cell with default membrane parameters. Generation of repetitive firing occurs above approximately -1.74 pA injected current.

Hyperpolarization activated current elicited after depolarization

Pyramidal cell action potentials elicited by disinhibition proved to be crucial for the timing of pyramidal cell activity (see Fig. 2). We studied what intrinsic mechanisms contribute to the precise timing of pyramidal neurons. As I_h current was suspected to be responsible for the induction of the generation of action potentials through depolarizing overshoot, we focused our attention on the contribution of I_h current in action potential and burst generation (Fig. 5). Furthermore, the question whether the dynamics of the I_h allows a single IPSC to elicit rebound activity or stronger and longer-lasting hyperpolarization is necessary for reliable rebound spikes was also asked.

Hyperpolarizing step currents were injected into the somatic compartment of the pyramidal cell model and conditions of rebound action potential generation were analyzed in the same compartment (Fig. 5*A*). To retain the same conditions that were used during simulations on basket cell network-inhibited pyramidal cell, the same tonic depolarization was applied to the soma of the pyramidal neuron. Furthermore, to have a clearer view on the direct effects of inhibition on pyramidal cell firing, we eliminated the spontaneously occurring action potentials of pyramidal cells by setting the sodium conductance of pyramidal neurons to 0 nS. The effect of intrinsic properties on action potential generation was evaluated by measuring the conditions necessary for reaching a predetermined action potential threshold (-52.6 mV). Although this threshold can vary dynamically

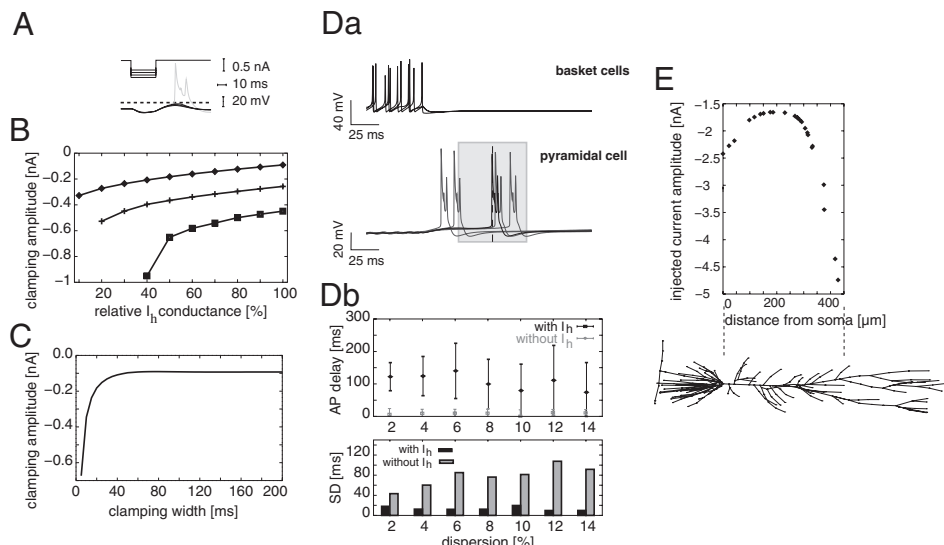


FIG. 5. Role of I_h in rebound spikes generation. *A*: typical membrane potential traces of the soma are shown (bottom) as a result of current clamping (top) the soma of the pyramidal cell. Solid lines on the top are subthreshold membrane potential traces, solid gray line is a suprathreshold trace, and dashed line is firing threshold. Clamping currents used were in the range of 0.05–0.15 nA; depolarizing current was 0.5 nA. *B*: increasing length of hyperpolarizing current pulse delivered to the soma of the pyramidal cell decreases strength of pulse necessary for reaching firing threshold. Necessary pulse strength saturates at ~ 40 ms. Depolarizing current was 0.55 nA. *C*: maximal conductance of I_h was systematically varied in the 10–100% interval, whereas minimal hyperpolarizing current pulse amplitude necessary to generate a DAP that reached the firing threshold was registered. Diamonds, crosses, and squares correspond to 0.60, 0.55, and 0.50 nA depolarization, respectively; pulse width was 40 ms. Decreased I_h conductance or decreased depolarization requires larger hyperpolarization for reaching firing threshold. *D*: enhancement of spiking reliability of pyramidal cells by the presence of I_h . *Da*: in applied protocol basket cell firing was suppressed after 1 s and time of pyramidal cell action potential occurrence relative to disinhibition was calculated. Dashed line: mean of pyramidal cell spike times. Shaded area: SD of spike times (SD). Variance of spike timing was result of random initial conditions and variance in the level of constant depolarization. *Db*: delay of pyramidal cell action potentials at different dispersion levels of pyramidal cell depolarizing current (top). In each case, delay is significantly larger when I_h is blocked but does not change with increasing dispersion. Furthermore, SD is remarkably larger without I_h (bottom). While SD does not increase with larger dispersion levels when I_h is present, it increases with I_h blocked. Convergence of basket cells on pyramidal cells was 20. *E*: top: minimal hyperpolarizing current eliciting rebound action potential as a function of distance measured from the soma. Depolarizing current of the pyramidal cell was set to 0 nA. Clamping time was set to 60 ms. Bottom: illustration of spatial dimensions of pyramidal cell used.

under physiological conditions (Azouz and Gray 2000), this does not affect the results shown here.

First, maximal conductance of the hyperpolarization-activated current was selectively and systematically varied at different depolarizing current levels (Fig. 5*B*). Simulation results showed that with decreased I_h , current conductance larger hyperpolarizing pulses were required to drive the pyramidal cell to the firing threshold. Below a given maximal conductance, firing threshold could not be reached in physiological circumstances at a given depolarizing current. Similar results could be obtained in simulations with intact sodium currents but without tonic depolarizing current on pyramidal cells. The only difference was a significantly higher depolarization needed for eliciting action potential in the pyramidal neuron (data not shown).

Next, we measured the minimal strength of the hyperpolarizing current step necessary to depolarize the pyramidal cell to the firing threshold at different pulse widths (Fig. 5*C*). At short hyperpolarization widths (<30 ms), the strength of the hyperpolarization increased steeply and saturated at about 40 ms at a level of 0.1 nA, when the pyramidal depolarization was 0.5 nA. Although basket cell IPSCs can be as high as 0.1 nA (Maccaferri et al. 2000), the duration is shorter than required for rebound burst generation. Therefore loosely synchronized IPSCs are required for eliciting rebound activity.

We tested explicitly whether hyperpolarization-activated current enhances precision of pyramidal cell spike timing. Pyramidal cells innervated by multiple basket cells were simulated with and without I_h . Firing rate of pyramidal neurons

was set inhomogeneously by setting their constant depolarization levels according to a Gaussian distribution. Postinhibitory facilitation of pyramidal cell spikes was probed by suppressing action potentials of all presynaptic basket cells and measuring both the delay and dispersion of pyramidal cell spikes (Fig. 5*Da*). Delay of action potentials was shown to be significantly larger when I_h was present at all dispersion levels (Fig. 5*Db*). Similarly, SD of action potential times was severalfold higher without I_h . Increase of dispersion, however, did not affect the average delay of action potentials in either case (Fig. 5*Db*). In contrast, SD increased with increasing dispersion when I_h was blocked but not when I_h was intact, showing that I_h greatly increases reliability of pyramidal cell timing when heterogeneity disrupts synchronous firing.

There is a trade-off between the level of hyperpolarization-activated conductance and the site of inhibition: with increasing distance from the soma the depolarizing sag elicited by disinhibition becomes larger but this pyramidal response is attenuating toward the soma. To quantify this trade-off, we conducted simulations, where the apical dendrite was stimulated at increasing distances from the soma (Fig. 5*E*). Simulations have shown that at the proximal apical dendrite after an initial decrease in the minimal pulse necessary to elicit action potential, the necessary pulse amplitude increased substantially beyond ~ 250 μ m. These results confirm that, despite that hyperpolarization-activated conductance is low in the soma and proximal dendrites of pyramidal cells, it contributes effectively to postinhibitory depolarization of pyramidal neurons.

Characteristics of theta oscillation

After examining pairwise interactions between neuron populations, we studied the performance of the interconnected three-population network. Connectivity and physiological parameters between neuron populations were set according to the results of the pairwise simulation studies (see METHODS for the specific values). The hippocampal circuitry formed by pyramidal cells and two classes of interneurons was able to generate theta-frequency oscillation as reflected by the firing histograms (Fig. 6A) and the extracellular field potential calculated from the activity of pyramidal neurons (Fig. 6B; see METHODS). To faithfully follow the protocol applied *in vitro*, synaptic transmission through AMPA synapses was suppressed. Firing histograms of all neuron populations showed theta-frequency modulation, but spike trains of individual pyramidal cells exhibited variability: they either fired spikes regularly in each theta cycle, or skipped a whole cycle (Fig. 6). Average period of firing of neuron populations was 51 ± 15 , 118 ± 18 , and 284 ± 42 ms for basket cells, O-LM cells, and pyramidal cells, respectively. We tested how activity of pyramidal cells affects the frequency of the population oscillation; therefore the depolarizing current injected into the soma of pyramidal cells was

systematically varied. Simulations revealed a monotonous increase in field potential theta frequency over a wide range of tonic depolarizing current levels (Fig. 6E). Behavior of separate cells was described in two ways: autocorrelation functions of individual membrane-potential traces were calculated (Fig. 6, C and D), and description of population activity was given by calculating the average frequency from the position of membrane potential power spectra peaks resulting from multiple trials (Fig. 6E, dashed line). The difference between frequencies of population activity and frequencies derived from individual neurons reveals that pyramidal cells do not necessarily fire action potentials in each cycle; rather, they skip cycles.

Because depolarization level of pyramidal cells has an effect on theta frequency, we studied whether the oscillation is robust against variations in this factor. We set the depolarizing current inhomogeneously, that is, while injecting constant current into pyramidal cells the strength of this current was determined randomly. Strength of injected current was picked from a Gaussian distribution with a given mean and SD was 3, 5, or 10%. Simulations confirmed that this kind of irregularity cannot disrupt the synchronization of cell populations (Fig. 6F). Changes in resting membrane potentials of pyramidal cells,

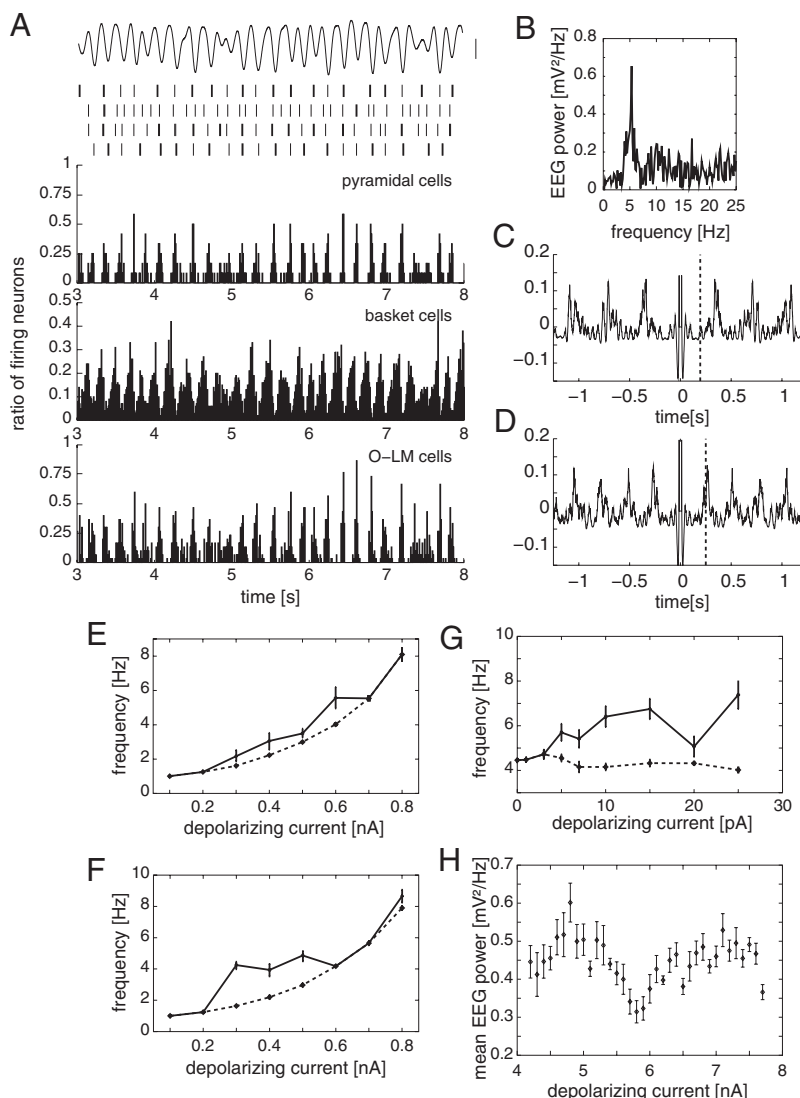


FIG. 6. Characterization of the theta frequency population oscillation using the 3-population network model. *A*: firing histograms of neuron populations show theta-frequency clustering of spikes. *Top*: low-pass filtered (15 Hz) extracellular field potential. Ticks: sample spike trains of 4 randomly chosen pyramidal cells. *B*: power spectrum of extracellular field potential shows a peak at 5 Hz. *C* and *D*: autocorrelation function of 2 randomly chosen pyramidal cells at 0.5- and 0.6-nA inducing current, respectively. Dashed line: period of theta oscillation, calculated from the EEG power. Note, that 1st peak in the autocorrelation function, reflecting period of action potential firing, does not coincide with frequency of population oscillation. *E* and *F*: mean frequency of theta activity as a function of depolarization of pyramidal cells. Level of depolarization was either set homogeneously at each pyramidal cell (*E*) or was picked from a Gaussian distribution with a mean indicated on the *y*-axis and SD of 5% (*F*). Solid line: mean frequency calculated from position of peak on power spectrum of low-pass filtered (1–15 Hz) EEG. Dashed line: mean frequency calculated from position of peak on power spectrum of membrane potential traces of individual pyramidal cells, averaged over different trials ($n = 8$). *G*: mean EEG frequency as a function of O-LM cell depolarization. Line types as above. A clear tendency of increasing population oscillation frequency with increasing pyramidal cell depolarization is remarkable, whereas only a moderate increase characterizes the similar manipulation of O-LM cells. *H*: dependence of synchronization efficacy on depolarization of pyramidal cells. Simulations were performed with inhomogeneous depolarization at both pyramidal cells (SD was 3%) and O-LM cells. Two separate intervals can be distinguished on the basis of high peak in power spectrum corresponding to 1:1 and 1:2 frequency synchronization of O-LM cells and pyramidal cells. Error bars denote SE; number of simulations at each depolarization level was 10.

i.e., scattering the reversal potential of the leakage current according to a Gaussian distribution, did not disrupt theta frequency oscillation either (data not shown).

Similarly, we tested whether altered firing properties of O-LM neurons can affect the frequency of population oscillation by injecting a small constant depolarizing current to each O-LM cell. Theta frequency, however, was only slightly affected by this altered O-LM cell behavior (Fig. 6G). Mean frequency of action potentials of individual pyramidal cells did not change but mean frequency of EEG showed an increasing tendency with increased depolarization. Synchronization of the network was tested with sparser pyramidal cell to O-LM cell connections. For this, we used larger number of pyramidal cells while keeping the convergence of pyramidal cells on O-LM cells constant (2.4). We used 15, 30, and 45 pyramidal neurons. Simulations showed that the power of theta did not change significantly with this modification (power of theta was 0.41 ± 0.04 , 0.35 ± 0.06 , and 0.38 ± 0.04 mV^2/Hz at 550-pA pyramidal cell depolarizing current, respectively).

Level of pyramidal cell depolarization affects the frequency of synchronization of neuron populations. Study of pyramidal cell-to-O-LM cell connections has revealed that efficacy of coupling of action potentials could only be achieved in narrow intervals and depended on the frequency of the action potentials of pyramidal neurons (Fig. 4). We performed simulations to explore how the depolarization of pyramidal cells affects synchronization properties of the network. Simulations with increasing pyramidal cell depolarization have shown that strong synchronization states are alternating with weak synchronization states (Fig. 6H). The two strong synchronization states correspond to the 1:1 and 1:2 frequency ratios of O-LM cells and pyramidal cells.

Firing histograms indicated that the preferred phases of neuron populations are locked to each other. Firing phase histograms, which relate firings of neurons to the phase of extracellular theta activity (Fig. 7A) revealed a nearly equal mean firing phase of the pyramidal cell population and O-LM cell population with a $2.2 \pm 1.9^\circ$ lag of pyramidal cells. Basket cells preceded pyramidal cells by $127.2 \pm 3.5^\circ$. Comparing results obtained for different pyramidal cell depolarization levels, i.e., different frequencies, a similar phase relationship could be established (Fig. 7B).

To check whether a possible basket cell-to-O-LM cell projection affects the relative timing of neuron populations, we performed simulations with different convergence of basket cells on O-LM neurons. For simplicity, dynamics of synapses connecting basket cells to O-LM cells were the same as those connecting basket neurons; maximal synaptic conductance was 0.88 nS. Up to a convergence of 30, simulations did not show any significant difference in the delay of neither basket cells nor pyramidal cells relative to O-LM neurons (data not shown).

Role of hyperpolarization-activated current in the population oscillation

Simulations were performed to test whether depolarizing afterpotentials evoked by the activation of hyperpolarization-activated current indeed support the synchronization of the network. Therefore we studied the case when depolarization of pyramidal cells was dispersed to simulate pyramidal cells with different firing rate, whereas conductance of I_h at different

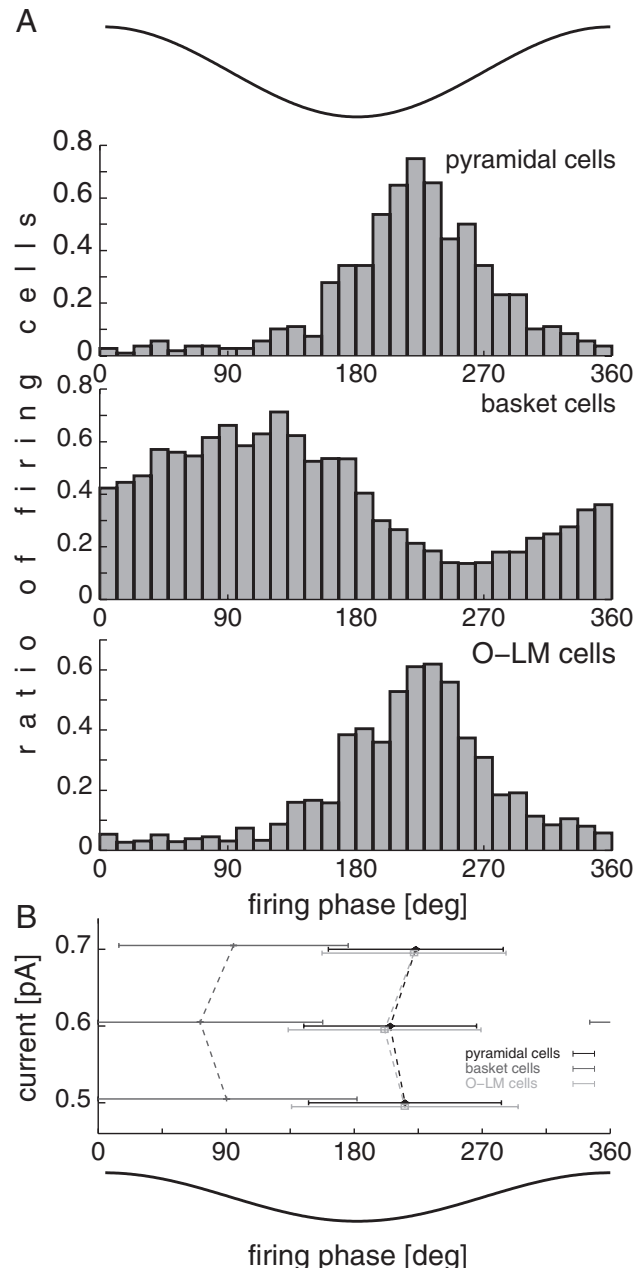


FIG. 7. Action potential timing of different cell populations relative to extracellular theta oscillation. **A:** phase distribution histograms (PDHs) of neuron populations. **Top:** demonstration of a field theta oscillation epoch. While pyramidal cells and O-LM cells have maxima in their PDHs at approximately the same phase, basket cells show an earlier maximum. Circular mean and angular deviation for pyramidal cells, basket cells, and O-LM cells were 223 ± 59 , 95 ± 81 , and $222 \pm 64^\circ$, respectively. **B:** PDH means and angular deviations at 3 different levels of pyramidal cell depolarization. Different gray levels denote different neuron populations. For better visibility, error bars belonging to different populations are shifted vertically.

network components was changed. In the model framework, I_h was present both in pyramidal cells and O-LM interneurons. First, I_h conductance was set to 0 pS at both populations. Eliminating I_h caused theta-frequency modulation of neuron populations to disappear (Fig. 8A). Parallel to this, the attenuation of the theta peak in the power spectrum of the EEG was remarkable (Fig. 8B). Comparison of control simulations and simulations performed without I_h conductance shows a signif-

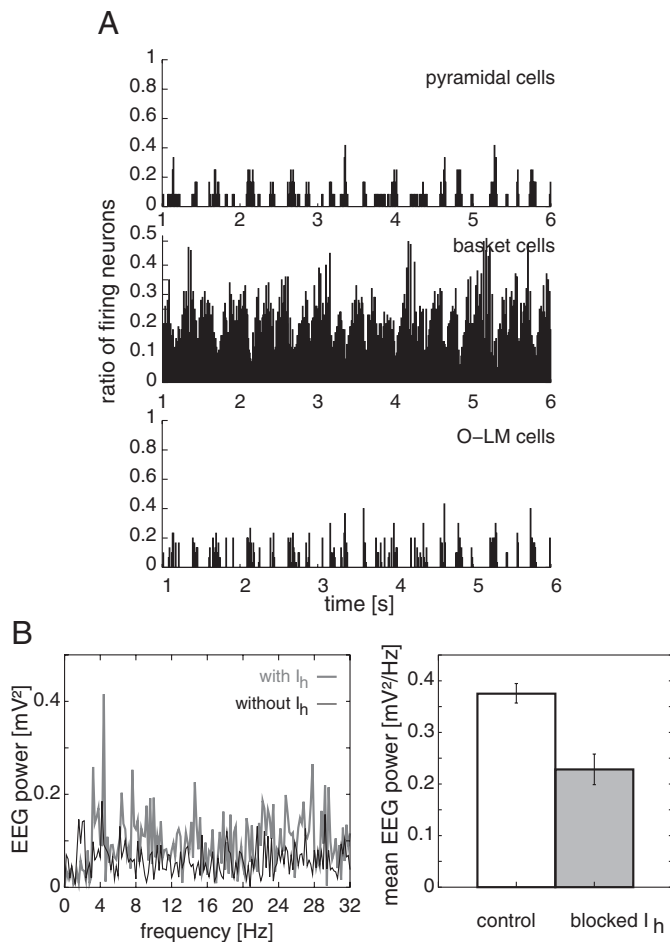


FIG. 8. Contribution of I_h to theta oscillation. A: spike histograms of hippocampal CA1 neuron populations when I_h is not present and frequencies of individual pyramidal cells are heterogeneous because of dispersed somatic depolarizing current (mean and SD of depolarization current was 0.62 and 0.03 nA, respectively). B and C: effect of I_h on network behavior, comparison of control with blocked I_h case. In control situation, I_h conductance was set to its default value, whereas blockade of I_h meant to set its maximal conductance to 0 pS. Depolarization of pyramidal cells was different for each cell; its level was picked from a Gaussian distribution. Simulations testing contribution of I_h were performed with blocked I_h conductance at both cells types. Power spectrum of the calculated EEG in B shows a decrease of theta-band (3–8 Hz) oscillation. Theta power decreases significantly when I_h current is totally blocked (gray bar) in the whole network compared with power in network with intact I_h (C), $P < 0.01$. Error bars denote SE.

icant drop in theta power (Fig. 8C). Contribution of I_h was also studied by reducing I_h conductance selectively at pyramidal cells and O-LM interneurons. Simulations have shown that reducing I_h at O-LM interneurons does not result in reduced theta amplitude (0.38 ± 0.09 compared with 0.38 ± 0.05 mV²/Hz in the control situation). However, a reduction of 55% was observable at simulations performed with blocked I_h at pyramidal cells (0.17 ± 0.04 mV²/Hz, while the mean amplitude was 0.23 ± 0.07 mV²/Hz with blocking at both sites).

Effects of glutamatergic transmission components

We studied network performance while different components of glutamatergic transmission were changed separately. Previously, theta has been shown to emerge in a CA1 slice when AMPA transmission was suppressed, whereas NMDA

transmission proved to be necessary for this kind of theta (Gillies et al. 2002). Theta could emerge in our network when the only excitatory synaptic transmission was realized by NMDA synapses (Figs. 6 and 7). Including AMPA receptor-mediated synaptic currents did not alter the power of theta oscillation significantly (in this case convergence of pyramidal cells on basket cells was 7). However, a significant increase was observed in the power at the gamma frequency band (20–80 Hz; 0.32 ± 0.13 mV²/Hz without and 0.87 ± 0.16 mV²/Hz with AMPA receptors). Increased excitation of basket cells caused by stronger pyramidal basket cell coupling resulted in more action potentials synchronized in gamma frequency, which in turn generated more synchronous IPSPs at target pyramidal cells. This subthreshold oscillation resulted in a gamma-frequency peak in the power spectrum of the extracellular field potential. This observation was further confirmed by the fact that increasing the convergence of pyramidal cells on basket neurons resulted in higher gamma activity (Fig. 9A). At higher convergence levels, the power of gamma-band activity could grow higher than the power of theta oscillation. The same increase in gamma power was achieved by increasing the conductance at AMPA synapses while keeping the convergence at a constant level. In this case, however, when AMPA was present both on O-LM cells and basket cells, there was an increase in the power (an increase of 30% with doubling the maximal synaptic conductance of AMPA), but not in the frequency of theta oscillation (data not shown).

We checked whether the enhanced gamma-band activity could be explained by enhancing the fast glutamatergic transmission between pyramidal cells and basket cells. Therefore simulations were performed where AMPA was blocked at pyramidal cell-to-O-LM cell synapses but was intact at pyramidal cell-to-basket cell synapses (Fig. 9B). Simulations have shown that enhanced pyramidal cell-to-basket cell synapses can account for increased power of gamma band activity when AMPA receptors are not blocked.

DISCUSSION

This study aimed at providing evidence using the compartmental modeling technique that the circuitry of hippocampal region CA1 is endowed with the ability to internally generate theta-frequency population oscillation with timing of neuron populations matching experimentally measured values. Preferred phase of neuron population firing was shown to be determined by the interactions between the populations. Timing of basket cell peak firing phase was set by the inhibition deriving from O-LM neurons. Simultaneous suppression of basket cell activity by a hyperpolarizing current step elicited action potentials in target pyramidal neurons with a mean latency of 20 ms, which grew as high as 60 ms when suppression of basket cells was achieved by IPSPs of O-LM neurons. Passive membrane properties and intrinsic theta-frequency firing of O-LM neurons enabled them to respond immediately to the excitation delivered by recurrent axons of pyramidal cells. The network was robust against heterogeneity in network structure, as reflected by the random connection patterns, and against heterogeneity in frequencies of individual pyramidal cells, as reflected by randomly set depolarizing currents. We propose that timing and thus synchronization of pyramidal cells is brought about by rebound spikes, which are facilitated

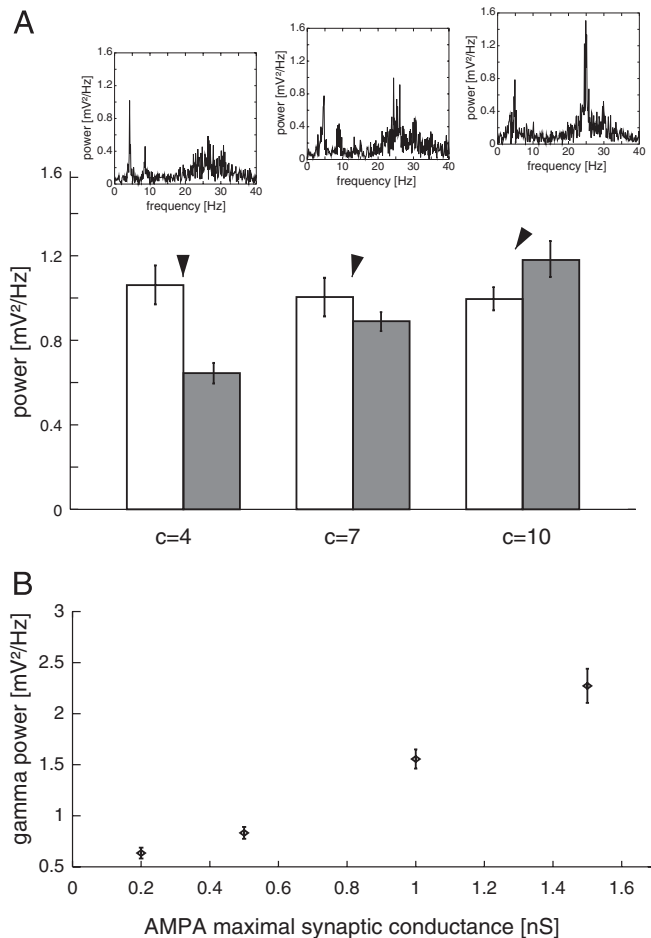


FIG. 9. Effect of AMPA receptor-mediated transmission on network oscillation. *A*: increased convergence (c) of pyramidal cells on basket interneurons enhances activity in the gamma band but not in the theta band. White bars show mean theta power, whereas gray bars show mean gamma power. *Insets*: sample power spectra at different convergence levels. With increasing convergence levels, gamma-band activity is enhanced. NMDA conductance at these simulations was 0.7 nS; AMPA conductance was 0.7 nS at both pyramidal cell-to-O-LM cell synapses and pyramidal cell-to-basket cell synapses. *B*: increased power of gamma band oscillation is caused by pyramidal cell-to-basket cell synapses. Increase of maximal synaptic conductance of AMPA synapses on basket cells causes increased power of the power spectrum in the gamma band. In these simulations, AMPA-mediated transmission was blocked at pyramidal cell-to-O-LM cell synapses; convergence of pyramidal cells on basket neurons was 7. Error bars denote SE. Depolarization of pyramidal cells was 0.71 nA throughout the simulations presented.

by the opening of hyperpolarization-activated nonspecific cation channels. We showed that the widely acknowledged role of NMDA conductance might rely on mechanisms intrinsic to the hippocampus and are effective in synchronizing the activity of hippocampal neurons.

Synchronization of neural populations

Synchronization can emerge in a network of neurons in different ways, e.g., by pacemaker neurons, which has been suggested in the visual cortex (Gray and McCormick 1996), by recurrent inhibition (van Vreeswijk et al. 1994; Wang and Buzsáki 1996; Wang and Rinzel 1993), in special cases recurrent excitation (Crook et al. 1998), and by activation of gap junctions (Traub 1995). The anatomical structure of the hip-

pocampus and the relatively slow time-course of theta oscillation (120–200 ms), however, impose constraints on the possible mechanisms. White et al. (2000) proposed that fast and slow GABA_A receptors expressed on distinct interneuron populations may contribute to theta activity. They have shown that a weak perforant path-mediated periodic input could organize discharges of the studied GABA cells in such a way that nested gamma (40–80 Hz) and theta oscillations emerged. The presented scenario might be beneficial in conditions when the perforant path input is intact, but it can neither account for theta when entorhinal cortex is removed by lesion (Buzsáki et al. 1983; Ylinen et al. 1995) nor for theta elicited in a CA1 slice (Gillies et al. 2002). Recently, Rotstein et al. (2005) described a mechanism of hippocampal CA1 theta generation in two populations of hippocampal interneurons, where fast-firing neurons innervated slow-firing neurons. In this study, theta-frequency synchronization is mainly driven by slow-firing oriens neurons, which give rise to slow IPSPs that silence the target basket cells for a longer period. Theta-frequency synchronization required the presence of I_h on oriens neurons. In the presented model, the authors assumed all-to-all connectivity, and it is not clear how the model would function under more realistic conditions, with sparser projections from one population to the other. Furthermore, the presented model does not give an account of the effects of glutamatergic transmission components. In our study, we showed that basket cell-to-OLM cell projections do not alter the relative timing of neuron populations during theta-frequency oscillation. However, as Rotstein et al. (2005) point out, this projection might have an effect on the stability of the network oscillation.

Another study highlighted the importance of the septohippocampal feedback (Wang 2002), showing an antiphase synchronization of medial septal GABAergic neurons and putative calbindin immunoreactive, I_h -containing interneurons. Here, the low-frequency synchronization was ensured by clusters of spikes fired by the septal neuron, which suppressed the firing of the hippocampo-septally projecting neurons for an interval comparable with the scale of theta oscillation. Septal phasic drive is an important component of the hippocampal theta but phase preferences of septal units are dispersed (King et al. 1998), and phase relationships of functional groups in the septum show an intricate pattern (Dragoi et al. 1999). If timing of hippocampal inhibitory neurons was achieved by periodic inhibition of these cells by medial septal GABAergic neurons, two problems would arise. First, although medial septal unit firing shows a hippocampal theta-locked behavior (King et al. 1998), preferred firing phases of these units are scattered over a broad interval (King et al. 1998). Second, medial septal units were shown to innervate hippocampal interneurons in a non-selective manner (Freund 1992), postsynaptic targets including both horizontal neurons with cell bodies in the oriens and basket cells; thus it would be hard to explain the difference between O-LM and basket cell firing phase preferences solely on the basis of medial septal interactions. These facts challenge the ultimateness of a scenario where synchrony is maintained by two neuron populations firing in an antiphase manner.

Hippocampal interneurons are known to quickly respond to excitation by emitting action potentials with high fidelity and release neurotransmitters with short latency (for review, see Jonas et al. 2004). This implies that in a pyramidal cell–O-LM neuron–basket cell chain, signals would propagate quickly; the

time needed would be much shorter than the characteristic time length of theta rhythm (120–300 ms). For measurable population activity, the synchronized activity of a high number of cells is required. Heterogeneity of synaptic connections, intrinsic cell parameters, and afferent activity, however, results in different excitability of individual cells. Hence population activity is built up on a longer time scale, and propagation of synchronized activity among neuron populations is slower than the propagation of a single signal between neurons of different populations. Earlier works (Kiss et al. 2001; Orbán et al. 2001) give a possible mechanism for the generation of this type of slow increase and decrease of population activity: activity of individual cells within the population synchronizes and desynchronizes during a theta cycle creating a population activity oscillation with theta frequency. In this study, we showed that propagation of synchronized activity through the proposed three-population system is realized in the period corresponding to the frequency of theta band (3–8 Hz).

We propose that phase relationships characteristic to hippocampal neuron populations during theta is determined by the intrahippocampal circuitry. According to the presented scenario, after prolonged suppression of pyramidal neurons by basket cells, rebound action potentials are fired in pyramidal neurons. These pyramidal neurons excite low-frequency firing O-LM cells through their recurrent axon collaterals. O-LM cells, in turn, inhibit a small number of basket neurons together with inhibiting distal apical dendrites of pyramidal cells. Theta-frequency synchronization is proposed to emerge in the loop formed by the three neuron populations.

Action potential timing of neuron populations

Precise timing of action potentials in hippocampal neurons is a crucial ingredient of hippocampal function. During exploratory behavior of rodents, theta oscillation constitutes a reference for action potentials of a subset of individual pyramidal cells, widely known as the phase precession effect (O'Keefe and Recce 1993; Skaggs et al. 1996). The cellular computation taking place in pyramidal cells for the phase precession to occur needs not only theta as a reference but synchronization of other neuron populations, e.g., interneurons, with each other (Lengyel and Érdi 2004; Lengyel et al. 2003).

Neural populations of the hippocampus were shown to be active at different phases of ongoing theta activity (Klausberger et al. 2003; Skaggs et al. 1996; Ylinen et al. 1995). While pyramidal cells and O-LM cells tend to have maximal firing probability at approximately the same time, maximal firing probability of basket cells precedes the former two by 110°, i.e., by 70 ms. Our simulations reproduced these results, showing that phase relationships of population activities are determined by pairwise interactions between them. These results are also consistent with the results of Gillies et al. (2002) on theta activity generated in a CA1 slice preparation. More specifically, we found that phasic coupling mediated through NMDA synapses between pyramidal cells and O-LM cells is capable of synchronizing these populations. This coupling results in the overlap between the population activities of O-LM cells and pyramidal neurons (Klausberger et al. 2003). The lag of pyramidal cells behind basket cells is compatible with the view that pyramidal cell bursts are generated because of disinhibition by basket interneurons (Buzsáki et al. 1983;

Cobb et al. 1995). Studies have shown that NMDA receptors have secondary effects by the interaction of NMDA receptors and metabotropic glutamate receptors (Alagarsamy et al. 1999). These nonphasic effects might also contribute to the maintaining of the theta oscillation in vitro, but it is shown in our paper that the weak phasic coupling between pyramidal cells and O-LM neurons is effective in synchronizing their activity (Fig. 4).

It is known that in, behaving rats, only a portion of pyramidal cells are active during a theta cycle (<3%) (Csicsvári et al. 1998, 1999), and activity of individual pyramidal cells is highest in a specific segment of the environment, called the place field of the respective neuron (O'Keefe and Dostrovsky 1971). Our model shed light on the function pyramidal cell firing might play in the synchronization and timing of coherent hippocampal theta rhythm. Synchronization based on a low fraction of active pyramidal cells is supported by the finding that pyramidal layer interneurons can be discharged by both single and dual presynaptic pyramidal cell spikes (Csicsvári et al. 1998). Based on anatomical data, oriens interneurons are better suited for collecting afferents coming from the recurrent collaterals of pyramidal cells (Freund and Buzsáki 1996). Taken together, this means that, despite the limited number of discharging place cells, pyramidal neurons can indeed pace a larger number of oriens interneurons, thus making synchronization in the theta band possible. In the presented model, only a fraction of CA1 pyramidal cells that were simulated as direct interaction among pyramidal cells is negligible because of their sparse recurrent collaterals. Modeled pyramidal cells represented only the few active pyramidal cells responsible for the synchronization of the population activity; thus these cells fired in almost every theta cycle. Although achieved only by a fraction of pyramidal cells, theta-modulated discharge of basket cells can maintain subthreshold theta-frequency oscillation in a large number of pyramidal cells as a result of the large divergence of basket cells (Freund and Buzsáki 1996; Sík et al. 1995).

Role of I_h in timing pyramidal cell action potentials

The hyperpolarization-activated current has a widely acknowledged role both in modulating passive properties of neurons, and participating in the generation of subthreshold and suprathreshold oscillations (Lüthi and McCormick 1998; Magee 1998; Pape 1996). Blockade of I_h was shown to delay subthreshold processes after hyperpolarizing current steps in lateral geniculate neurons (Lüthi et al. 1998), similarly to the observations made in this study. Furthermore, frequency modulation in heartbeat neurons of leech was shown to occur with varied I_h conductance (Olsen et al. 1995). More recently, resonance properties of hippocampal CA1 pyramidal neurons were probed with graded frequency input, and I_h was shown to contribute to theta-frequency response of pyramidal cells during hyperpolarization (Hu et al. 2002). The role of I_h in vivo is more controversial. Theta activity in hippocampus of mice was shown to be augmented when *HCN1* gene, a major component of I_h , was deleted (Nolan et al. 2004). In contrast with this study, Kitayama et al. (2002) showed a significant decrease in theta power after injection of cesium chloride, an I_h current blocker, in the apical dendritic layer of the hippocampal CA1 in vivo.

The question why theta is more robust with I_h than without it may arise naturally. Without I_h far from the firing threshold, the pyramidal cell soma works as a leaky integrate and fire neuron, that is, after releasing from a hyperpolarized state receiving tonic depolarization its membrane potential converges toward a given membrane potential, and if this membrane potential is above the firing threshold, a spike is generated. The slope of membrane potential increase is determined by multiple factors, including resting membrane potential, synaptic inputs, passive membrane characteristics, and depolarization. Heterogeneity of these factors in the pyramidal cell population results in a considerable variance of the slope, hence the frequency of action potential and burst generation. Consequently, diversity of neurons in a certain population means a force that tends to desynchronize the activity of that population. Indeed, our simulations have shown that this frequency variation causes a significant drop in theta power when I_h is blocked.

Presence of I_h enables basket neurons to restrict pyramidal cells to fire action potentials in a narrow time window after disinhibition. Slow deactivation of I_h results in a postinhibitory sag, which effectively gates pyramidal cell firing. Timing of pyramidal cell activity has previously been shown to be brought about by inhibitory gating (Cobb et al. 1995), but the identity of membrane currents generating the postinhibitory sag was not exclusively determined. Our findings show that physiologically realistic distribution and activation and deactivation characteristics of I_h on pyramidal cells (Magee 1998) are effective in timing rebound action potentials. Furthermore, we have shown that basket cells preferentially innervating the somatic region of pyramidal cells (Freund and Buzsáki 1996) are good candidates for mediating the inhibition necessary for I_h activation. Also, because the perisomatic membrane area is rich in sodium channels depolarization initiated by the activation of I_h could result in action potential or burst generation. In contrast, with previous suggestions (Gillies et al. 2002), we found that the presence of I_h was not necessary, although beneficial, at O-LM neurons for extracellularly measurable theta. However, intact I_h at pyramidal cells was essential for synchronization in theta frequency band.

NMDA receptors are effective in theta-band synchronization

NMDA receptors were hypothesized to be crucial in the generation of theta activity in behaving animals (Buzsáki 2002). Furthermore, theta generated in a CA1 slice has also been shown to depend on glutamatergic transmission through NMDA receptors (Gillies et al. 2002). We showed that the circuitry expressing NMDA receptors on O-LM neurons is capable of synchronizing activity in the theta band. Indeed, in their study, Nyíri et al. (2003) have shown that NMDA receptors in the hippocampal CA1 reside dominantly on O-LM neurons rather than basket neurons. Because these neuron populations have been shown to be the target of pyramidal cells (Blasco-Ibanez and Freund 1995; Ali et al. 1998; Lacaille et al. 1987) in a hippocampal CA1 slice, the main excitatory drive using NMDA receptors is presumed to innervate O-LM neurons. In contrast, the effect of non-NMDA glutamatergic receptors was shown to be twofold *in vitro* (Gillies et al. 2002). On one hand, application of NBQX decreased gamma-band activity, an observation reproduced by blocking AMPA recep-

tor-mediated synaptic transmission in our model. We have shown that increased excitation of basket cells might underlie stronger gamma-band activity: enhanced transmission at pyramidal cell-to-basket cell synapses or richer pyramidal cell-to-basket cell projections resulted in concomitant increase in gamma power. On the other hand, theta-band activity was only significant with application of NBQX. Including the AMPA receptors in our network model caused stronger gamma-band activity than theta-band activity, but theta was not abolished. We hypothesize that this difference between simulation performance and experiment is a consequence of other, not modeled, interneuron populations rich in AMPA receptors and recurrent synapses from CA1 pyramidal neurons (Ali et al. 1998; Buhl et al. 1994). In summary, the unbalanced expression of NMDA and AMPA receptors on basket and O-LM neurons can account for the requirement of AMPA receptor block for reduced gamma activity *in vitro*.

Entorhinal cortical modulation of theta activity

In *in vivo* conditions, the hippocampal CA1 receives phasic theta-frequency drive from the CA3, entorhinal cortex (Chrobak and Buzsáki 1998), and neurons in the septum also fire in phase with hippocampal theta (King et al. 1998). Therefore *in vivo*, the current generators of theta in the CA1 region are manifold (Buzsáki 2002). Depth profile of theta activity shows a remarkable peak near the lacunosum moleculare, suggesting that the entorhinal cortex indeed exerts periodic excitation on CA1 pyramidal cells (Bragin et al. 1995; Ylinen et al. 1995). This is further confirmed by the presence of sinks in current source density maps in lacunosum moleculare (Kamondi et al. 1998). The contribution of perforant path-mediated excitation can be elucidated by analyzing data from entorhinal lesion experiments (Bragin et al. 1995), which shows that theta is present after entorhinal cortical lesion but the power is reduced at distal apical dendritic region corresponding to the region where perforant path terminates. Lesion leads to a depth profile of theta phase similar to theta observed in urethane anesthetized rats (Ylinen et al. 1995). A salient characteristic of CA1 theta is a lower frequency synchronization of neuron populations during anesthesia (Vanderwolf et al. 1977). Comparing these data with our results, one can conclude that entorhinal cortical input interacts with theta generated internally in the hippocampal CA1, pacing a higher frequency oscillation. Also, entorhinal cortex has to have a role in modulating hippocampal neuronal activity to participate in the generation and maintenance of phase codes (Harris et al. 2002; O'Keefe and Recce 1993). Synchronization of hippocampal neuron populations, however, does not need external phasic input and timing of hippocampal neuron populations relies on the internal structure of the hippocampal circuitry.

One of the most prominent feature of O-LM neurons is their axon arborization pattern. Axons emerging from the stratum oriens show arborization in the stratum moleculare and are coaligned with perforant path synapses (Sik et al. 1995). Because perforant path input was not considered in this study, the possible regulatory role of O-LM synapses was not studied either. Because of the distant position of O-LM cell synapses, it seems plausible that O-LM cells exert their full power in regulation of perforant path rather than directly controlling the output of pyramidal cells. Indeed, theoretical studies indicate

that O-LM cells are ideally suited for filtering perforant path input for performing computations in the hippocampus (Lengyel and Érdi 2004). It remains the subject of further studies to elucidate the precise interactions between hippocampal, entorhinal cortical, and other cortical oscillations *in vivo*.

ACKNOWLEDGMENTS

The authors thank M. Lengyel, M. Hajós, and H. Rotstein for helpful discussions, G. Debreczeni for technical assistance at the RMKI LCG Center, and G. Csárdi for extending the GENESIS software for Grid computing.

GRANTS

This work was supported by a grant from the Hungarian Scientific Research Fund (T038140) and the Henry R. Luce Foundation.

REFERENCES

Alagarsamy S, Marino MJ, Rouse ST, Gereau RW IV, Heinemann SF, and Conn PJ. Activation of NMDA receptors reverses desensitization of mGluR5 in native and recombinant systems. *Nat Neurosci* 2: 234–240, 1999.

Ali AB, Deuchars J, Pawelzik H, and Thomson AM. CA1 pyramidal to basket and bistratified cell EPSPs: dual intracellular recordings in rat hippocampal slices. *J Physiol* 507: 201–217, 1998.

Ali AB and Thomson AM. Facilitating pyramid to horizontal oriens-alveus interneurone inputs: dual intracellular recordings in slices of rat hippocampus. *J Physiol* 507: 185–199, 1998.

Alonso A, Gaztelu JM Jr, Buno W, and Garcia-Austt E. Cross-correlation analysis of septohippocampal neurons during theta-rhythm. *Brain Res* 413: 135–146, 1987.

Azouz R and Gray CM. Dynamic spike threshold reveals a mechanism for synaptic coincidence detection in cortical neurons *in vivo*. *Proc Natl Acad Sci USA* 97: 8110–8115, 2000.

Baude A, Nusser Z, Molnár E, McIlhinney RA, and Somogyi P. High-resolution immunogold localization of AMPA type glutamate receptor subunits at synaptic and non-synaptic sites in rat hippocampus. *Neuroscience* 69: 1031–1055, 1995.

Bland BH, Oddie S, and Colom L. Mechanisms of neural synchrony in the septohippocampal pathways underlying hippocampal theta generation. *J Neurosci* 19: 3223–3237, 1999.

Blasco-Ibanez JM and Freund TF. Synaptic input of horizontal interneurons in stratum oriens of the hippocampal CA1 subfield: structural basis of feed-back activation. *Eur J Neurosci* 7: 2170–2180, 1995.

Bragin A, Jandó G, Nádasdy Z, Hetke J, Wise K, and Buzsáki G. Gamma (40–100 Hz) oscillation in the hippocampus of the behaving rat. *J Neurosci* 15: 47–60, 1995.

Buhl EH, Han ZS, Lorinczi Z, Stezhka VV, Karnup SV, and Somogyi P. Physiological properties of anatomically identified axo-axonic cells in the rat hippocampus. *J Neurophysiol* 71: 1289–1307, 1994.

Bullock TH, Buzsáki G, and McClune MC. Coherence of compound field potentials reveals discontinuities in the CA1-subiculum of the hippocampus in freely-moving rats. *Neuroscience* 38: 609–619, 1990.

Buzsáki G. Theta oscillations in the hippocampus. *Neuron* 33: 325–340, 2002.

Buzsáki G, Leung LW, and Vanderwolf CH. Cellular bases of hippocampal EEG in the behaving rat. *Brain Res* 287: 139–171, 1983.

Chapman CA and Lacaille JC. Intrinsic theta-frequency membrane potential oscillations in hippocampal CA1 interneurons of stratum lacunosum-moleculare. *J Neurophysiol* 81: 1296–1307, 1999.

Chrobak JJ and Buzsáki G. Operational dynamics in the hippocampal-entorhinal axis. *Neurosci Biobehav Rev* 22: 303–310, 1998.

Cobb S, Buhl EH, Halasy K, Paulsen O, and Somogyi P. Synchronization of neuronal activity in hippocampus by individual GABAergic interneurons. *Nature* 378: 75–78, 1995.

Crook SM, Ermentrout GB, and Bower JM. Spike frequency adaptation affects the synchronization properties of networks of cortical oscillations. *Neural Comput* 10: 837–854, 1998.

Csicsvári J, Hirase H, Czurkó A, and Buzsáki G. Reliability and state dependence of pyramidal-interneuron synapses in the hippocampus: an ensemble approach in the behaving rat. *Neuron* 21: 179–189, 1998.

Csicsvári J, Hirase H, Czurkó A, Mamiya A, and Buzsáki G. Oscillatory coupling of hippocampal pyramidal cells and interneurons in the behaving rat. *J Neurosci* 19: 274–287, 1999.

Destexhe A, Mainen Z, and Sejnowski TJ. Kinetic models of synaptic transmission. In: *Methods in Neuronal Modeling* (2nd ed.), edited by Koch C and Segev I. Cambridge, MA: MIT Press, 1998, p. 1–25.

Dragoi G, Carpi D, Recce M, Csicsvári J, and Buzsáki G. Interactions between hippocampus and medial septum during sharp waves and theta oscillation in the behaving rat. *J Neurosci* 19: 6191, 1999.

Fox SE. Membrane potential and impedance changes in hippocampal pyramidal cells during theta rhythm. *Exp Brain Res* 77: 283–294, 1989.

Freund TF, GABAergic septal and serotonergic median raphe afferents preferentially innervate inhibitory interneurons in the hippocampus and dentate gyrus. *Epilepsy Res Suppl* 7: 79–91, 1992.

Freund TF and Buzsáki G. Interneurons of the hippocampus. *Hippocampus* 6: 347–470, 1996.

Gillies MJ, Traub RD, LeBeau FEN, Davies CH, Gloveli T, Buhl EH, and Whittington MA. A model of atropine-resistant theta oscillations in rat hippocampal area CA1. *J Physiol* 543: 779–793, 2002.

Gray CM and McCormick DA. Chattering cells: superficial pyramidal neurons contributing to the generation of synchronous oscillations in the visual cortex. *Science* 274: 109–113, 1996.

Gulyás AI, Hajós N, Katona I, and Freund TF. Interneurons are the local targets of hippocampal inhibitory cells which project to the medial septum. *Eur J Neurosci* 17: 1861–1872, 2003.

Gulyás AI, Miles R, Hajós N, and Freund TF. Precision and variability in postsynaptic target selection of inhibitory cells in the hippocampal CA3 region. *Eur J Neurosci* 5: 1729–1751, 1993a.

Hajós M, Hoffmann WE, Orbán G, Kiss T, and Érdi P. Modulation of septo-hippocampal theta activity by GABA_A receptors: an experimental and computational approach. *Neuroscience* 126: 599–610, 2004.

Hajós N and Mody I. Synaptic communication among hippocampal interneurons: properties of spontaneous IPSCs in morphologically identified cells. *J Neurosci* 17: 8427–8442, 1997.

Harris KD, Henze DA, Hirase H, Leinekugel X, Dragoi G, Czurkó A, and Buzsáki G. Spike train dynamics predicts theta-related phase precession in hippocampal pyramidal cells. *Nature* 417: 738–741, 2002.

Hu H, Vervaeke K, and Storm JF. Two forms of electrical resonance at theta frequencies, generated by M-current, h-current and persistent Na⁺ current in rat hippocampal pyramidal cells. *J Physiol* 545: 783–805, 2002.

Jonas P, Bischofberger J, Fricker D, and Miles R. Interneuron diversity series: fast in, fast out-temporal and spatial signal processing in hippocampal interneurons. *Trends Neurosci* 27: 30–40, 2004.

Kamondi A, Acsády L, Wang XJ, and Buzsáki G. Theta oscillations in somata and dendrites of hippocampal pyramidal cells *in vivo*: activity-dependent phase-precession of action potentials. *Hippocampus* 8: 244–261, 1998.

Katona I, Acsády L, and Freund TF. Postsynaptic targets of somatostatin-immunoreactive interneurons in the rat hippocampus. *Neuroscience* 88: 37–55, 1999.

King C, Recce M, and O'Keefe J. The rhythmicity of cells of the medial septum/diagonal band of Broca in the awake freely moving rat: relationships with behaviour and hippocampal theta. *Eur J Neurosci* 10: 464–477, 1998.

Kiss T, Orbán G, Lengyel M, and Érdi P. Intrahippocampal gamma and theta rhythm generation in a network model of inhibitory interneurons. *Neurocomputing* 38–40: 713–719, 2001.

Kitayama M, Taguchi T, Miyata H, Matsuda Y, Yamauchi T, and Kogure S. The extracellular current blocking effect of cesium chloride on the theta wave in the rabbit hippocampal cal region. *Neurosci Lett* 334: 45–48, 2002.

Klausberger T, Magill PJ, Márton LF, Roberts JDB, Cobden PM, Buzsáki G, and Somogyi P. Brain-state- and cell-type-specific firing of hippocampal interneurons *in vivo*. *Nature* 421: 844–848, 2003.

Klausberger T, Márton L, Baude A, Roberts J, Magill P, and Somogyi P. Spike timing of dendrite-targeting bistratified cells during hippocampal network oscillations *in vivo*. *Nat Neurosci* 7: 41–47, 2004.

Knowles WD, Funch PG, and Schwartzkroin PA. Electrotomographic and dye coupling in hippocampal CA1 pyramidal cells *in vitro*. *Neuroscience* 7: 1713–1722, 1982.

Kocsis B, Bragin A, and Buzsáki G. Interdependence of multiple theta generators in the hippocampus: a partial coherence analysis. *J Neurosci* 19: 6200–6212, 1999.

Kuner T and Schoepfer R. Multiple structural elements determine subunit specificity of Mg²⁺ block in NMDA receptor channels. *J Neurosci* 16: 3549–3558, 1996.

Lacaille JC, Mueller AL, Kunkel DD, and Schwartzkroin PA. Local circuit interactions between oriens/alveus interneurons and CA1 pyramidal cells in

hippocampal slices: electrophysiology and morphology. *J Neurosci* 7: 1979–1993, 1987.

Lengyel M and Érdi P. Theta-modulated feed-forward network generates rate and phase coded firing in the entorhino-hippocampal system. *IEEE Trans Neural Network* 15: 1092–1099, 2004.

Lengyel M, Szatmáry Z, and Érdi P. Dynamically detuned oscillations account for the coupled rate and temporal code of place cell firing. *Hippocampus* 13: 700–714, 2003.

Lopes da Silva FH, Witter MP, Boeijinga PH, and Lohman AH. Anatomic organization and physiology of the limbic cortex. *Physiol Rev* 70: 453–511, 1990.

Lüthi A, Bal T, and McCormick DA. Periodicity of thalamic spindle waves is abolished by ZD7288, a blocker of I_h . *J Neurophysiol* 79: 3284–3289, 1998.

Lüthi A and McCormick DA. I_h -current: properties of a neuronal and network pacemaker. *Neuron* 21: 9–12, 1998.

Maccaferri G and McBain CJ. The hyperpolarization-activated current (I_h) and its contribution to pacemaker activity in rat CA1 hippocampal stratum oriens-alveus interneurons. *J Physiol* 497: 119–130, 1996.

Maccaferri G, Roberts JD, Szucs P, Cottingham CA, and Somogyi P. Cell surface domain specific postsynaptic currents evoked by identified GABAergic neurones in rat hippocampus *in vitro*. *J Physiol* 524: 91–116, 2000.

Magee J. Dendritic hyperpolarization-activated currents modify the integrative properties of hippocampal CA1 pyramidal neurons. *J Neurosci* 18: 7613–7624, 1998.

McBain CJ, DiChiara TJ, and Kauer JA. Activation of metabotropic glutamate receptors differentially affects two classes of hippocampal interneurons and potentiates excitatory synaptic transmission. *J Neurosci* 14: 4433–4445, 1994.

Mitchell SJ and Ranck J Jr. Generation of theta rhythm in medial entorhinal cortex of freely moving rats. *Brain Res* 189: 49–66, 1980.

Nolan MF, Malleret G, Dudman JT, Buhl DL, Santoro B, Gibbs E, Vronskaya S, Buzsáki G, Siegelbaum SA, Kandel ER, and Morozov A. A behavioral role for dendritic integration: HCN1 channels constrain spatial memory and plasticity at inputs to distal dendrites of CA1 pyramidal neurons. *Cell* 119: 719–732, 2004.

Nusser Z, Lujan R, Laube G, Roberts JD, Molnár E, and Somogyi P. Cell type and pathway dependence of synaptic AMPA receptor number and variability in the hippocampus. *Neuron* 21: 545–559, 1998.

Nyíri G, Stephenson FA, Freund TF, and Somogyi P. Large variability insynaptic N-methyl-D-aspartate receptor density on interneurons and a comparison with pyramidal-cell spines in the rat hippocampus. *Neuroscience* 119: 347–363, 2003.

O'Keefe J and Dostrovsky J. The hippocampus as a spatial map: preliminary evidence from unit activity in the freely-moving rat. *Brain Res* 34: 171–175, 1971.

O'Keefe J and Recce ML. Phase relationship between hippocampal place units and the EEG theta rhythm. *Hippocampus* 3: 317–330, 1993.

Olsen O, Nadim F, and Calabrese RL. Modeling the leech heartbeat elemental oscillator. II. Exploring the parameter space. *J Comput Neurosci* 2: 237–257, 1995.

Ongini E, Barzaghi C, and Marzanatti M. Intrinsic and antagonistic effects of beta-carboline fg 7142 on behavioral and eeg actions of benzodiazepines and pentobarbital in cats. *Eur J Pharmacol* 95: 125–129, 1983.

Orbán G, Kiss T, Lengyel M, and Érdi P. Hippocampal rhythm generation: gamma-related theta-frequency resonance in CA3 interneurons. *Biol Cybern* 84: 123–132, 2001.

Pape HC. Queer current and pacemaker: the hyperpolarization-activated cation current in neurons. *Annu Rev Physiol* 58: 299–327, 1996.

Pawelzik H, Hughes D, and Thomson AM. Physiological and morphological diversity of immunocytochemically defined parvalbumin- and cholecystokinin-positive interneurons in CA1 of the adult rat hippocampus. *J Comp Neurol* 443: 346–367, 2002.

Petsche H, Stumpf C, and Gogolak G. The significance of the rabbit's septum as a relay station between the mid-brain and the hippocampus. I. The control of hippocampal arousal activity by the septum cells. *EEG Clin Neurophysiol* 14: 202–211, 1962.

Rotstein HG, Pervouchine DD, Acker CD, Gillies MJ, White JA, Buhl EH, Whittington MA, and Kopell N. Slow and fast inhibition and an I_h -current interact to create a theta rhythm in a model CA1 interneuron network. *J Neurophysiol* 94: 1509–1518, 2005.

Sík A, Penttonen M, Ylinen A, and Buzsáki G. Hippocampal CA1 interneurons: an *in vivo* intracellular labeling study. *J Neurosci* 15: 6651–6665, 1995.

Skaggs WE, McNaughton BL, Wilson MA, and Barnes CA. Theta phase precession in hippocampal neuronal populations and the compression of temporal sequences. *Hippocampus* 6: 149–172, 1996.

Soltész I and Deschenes M. Low- and high-frequency membrane potential oscillations during theta activity in CA1 and CA3 pyramidal neurons of the rat hippocampus under ketamine-xylazine anesthesia. *J Neurophysiol* 70: 97–116, 1993.

Strata F. Intrinsic oscillations in CA3 pyramids: physiological relevance to theta rhythm generation. *Hippocampus* 8: 666–679, 1998.

Traub RD. Model of synchronized population bursts in electrically coupled interneurons containing active dendritic conductances. *J Comput Neurosci* 2: 283–289, 1995.

van Vreeswijk C, Abbott LF, and Ermentrout GB. When inhibition not excitation synchronizes neural firing. *J Comput Neurosci* 1: 313–321, 1994.

Vanderwolf CH, Buzsáki G, Cain D, Cooley RK, and Robertson B. Neocortical and hippocampal electrical activity following decapitation in the rat. *Brain Res* 451: 340–344, 1988.

Vanderwolf CH, Kramis R, and Robinson TE. Hippocampal electrical activity during waking behaviour and sleep: analyses using centrally acting drugs. *Ciba Found Symp* 58: 199–226, 1977.

Vértes RP and Kocsis B. Brainstem-diencephalo-septohippocampal systems controlling the theta rhythm of the hippocampus. *Neuroscience* 81: 893–926, 1997.

Wang XJ. Pacemaker neurons for the theta rhythm and their synchronization in the septohippocampal reciprocal loop. *J Neurophysiol* 87: 889–900, 2002.

Wang XJ and Buzsáki G. Gamma oscillation by synaptic inhibition in a hippocampal interneuron network model. *J Neurosci* 16: 6402–6413, 1996.

Wang XJ and Rinzel J. Spindle rhythmicity in the reticularis thalami nucleus: synchronization among mutually inhibitory neurons. *Neuroscience* 53: 899–904, 1993.

Warman EN, Durand DM, and Yuen GL. Reconstruction of hippocampal CA1 pyramidal cell electrophysiology by computer simulation. *J Neurophysiol* 6: 2033–2045, 1994.

White JA, Banks MI, Pearce RA, and Kopell NJ. Networks of interneurons with fast and slow γ -aminobutyric acid type a (GABA_A) kinetics provide substrate for mixed gamma-theta rhythm. *Proc Natl Acad Sci USA* 97: 8128–8133, 2000.

Williams JH and Kauer JA. Properties of carbachol-induced oscillatory activity in rat hippocampus. *J Neurophysiol* 78: 2631–2640, 1997.

Ylinen A, Soltész I, Bragin A, Penttonen M, Sík A, and Buzsáki G. Intracellular correlates of hippocampal theta rhythm in identified pyramidal cells, granule cells, and basket cells. *Hippocampus* 5: 78–90, 1995.